Stem Cell Reports
Article

ISSCR

OPEN ACCESS

# A Robust Single Primate Neuroepithelial Cell Clonal Expansion System for Neural Tube Development and Disease Studies

Xiaoqing Zhu,[1,3,6] Bo Li,[1,2,6] Zongyong Ai,[1,3,6] Zheng Xiang,[1,2] Kunshang Zhang,[5] Xiaoyan Qiu,[1] Yongchang Chen,[1,3] Yuemin Li,[2] Joshua D. Rizak,[4] Yuyu Niu,[1,3] Xintian Hu,[4] Yi Eve Sun,[1,5] Weizhi Ji,[1,3,*] and Tianqing Li[1,3,*]

[1]Yunnan Key Laboratory of Primate Biomedical Research, Institute of Primate Translational Medicine, Kunming University of Science and Technology, Kunming, 650500 Yunnan, China
[2]Chongqing Key Lab of Forage & Herbivore, College of Animal Science and Technology (CAST), Southwest University, No. 1 Tiansheng Road, Beibei, Chongqing 400715, China
[3]National Engineering Research Center of Biomedicine and Animal Science, Kunming 650500, China
[4]Kunming Institute of Zoology, Chinese Academy of Sciences, Kunming, 650223 Yunnan, China
[5]Translational Stem Cell Research Center, Tongji Hospital, Tongji University School of Medicine, Shanghai 200092, China
[6]Co-first author
*Correspondence: wji@kbimed.com (W.J.), litq@kbimed.com (T.L.)
http://dx.doi.org/10.1016/j.stemcr.2015.10.007


## SUMMARY

Developing a model of primate neural tube (NT) development is important to promote many NT disorder studies in model organisms. Here, we report a robust and stable system to allow for clonal expansion of single monkey neuroepithelial stem cells (NESCs) to develop into miniature NT-like structures. Single NESCs can produce functional neurons in vitro, survive, and extensively regenerate neuron axons in monkey brain. NT formation and NESC maintenance depend on high metabolism activity and Wnt signaling. NESCs are regionally restricted to a telencephalic fate. Moreover, single NESCs can turn into radial glial progenitors (RGPCs). The transition is accurately regulated by Wnt signaling through regulation of Notch signaling and adhesion molecules. Finally, using the "NESC-TO-NTs" system, we model the functions of folic acid (FA) on NT closure and demonstrate that FA can regulate multiple mechanisms to prevent NT defects. Our system is ideal for studying NT development and diseases.

## INTRODUCTION

Neural tube defects (NTDs) are still poorly understood, especially for human and non-human primates (NHPs) (Wallingford et al., 2013). In rhesus monkeys, at embryonic day 19–20 (E19–20), the neural tube (NT) contains multiple pseudostratified layers of neuroepithelial stem cells (NESCs) (Davignon et al., 1980). Proper cell division, establishment of polarity, and cell movement of NESCs are crucial for NT formation and NT closure (NTC) (Bush et al., 1990). However, abnormal growth of NESCs results in NTDs and, subsequently, defective brain development (Fish et al., 2006). During development, formation of the NT is a time-dependent transient event, difficult to capture, which limits study of it.

After NT formation, the NESC at E12 in mouse undergoes asymmetric divisions to generate one radial glial progenitor cell (RGPC), which exhibits residual neuroepithelial and astroglial properties (Kriegstein and Götz, 2003), and one migratory postmitotic daughter neuron (Kriegstein and Alvarez-Buylla, 2009). Thus, the transition of RGPCs is another fundamental event of brain development. Unfortunately, we still know very little about the RGPC transition process.

Previous reports have demonstrated differentiation of human embryonic stem cells (ESCs) into primitive neural precursor cells (NPCs) or neural rosette cells, which are composed of a myriad of cells along with anterior to posterior cell types (Elkabetz et al., 2008; Koch et al., 2009a; Li et al., 2011). A myriad of cells renders it difficult to study NT development and RGPC transition, even though a few cells maintain clonal expansion. In addition, a human pluripotent stem cells (PSCs)-derived three-dimensional organoid culture system, termed cerebral organoids, was developed to generate various discrete brain regions and could be used to model microcephaly (Lancaster et al., 2013). With the demonstration that the cortex and brain development can be recapitulated in vitro using stem cells (Espuny-Camacho et al., 2013; Lancaster et al., 2013), it is now conceivable that NTC could also be modeled in this way. Although a 3D neural tube system was recently established using embryonic bodies from mouse ESCs (Meinhardt et al., 2014), it is unclear whether the system can be used to model NTC and study NTDs. Furthermore, the system is unable to definitely control NESC self-renewal and differentiation as well as RGPC transition. Therefore, developing a simple culture system, which supports single-ESC-derived NESCs to self-organize into NT-like structures and model the RGPC transition in a stable, controlled, and conserved manner, will be rather advantageous to unveil molecular mechanisms underlying primate NTC and NTDs as well as NESC self-renewal mechanisms.

## RESULTS

### Rapid Generation of NESCs from Rhesus Monkey ESCs

In this study, NESCs were induced from rhesus monkey ESCs (rESCs) using a cocktail containing basic fibroblast growth factor (bFGF) (LaVaute et al., 2009); CHIR99021, a GSK3 inhibitor (Li et al., 2011; Lyashenko et al., 2011); SB431542, a transforming growth factor β (TGF-β) inhibitor (Chambers et al., 2009; Li et al., 2011); compound E, a Notch inhibitor (Li et al., 2011); and LDN193189, an inhibitor of ALK2 and ALK3 (Chambers et al., 2009). rESCs formed embryo bodies (EBs) with typical morphologies at post-differentiation day 2 (pdD2), which quickly formed a neuroepithelial cell layer, referred to as "neural bodies (NBs)," as confirmed by NESTIN staining at pdD5 or pdD6 (Figures 1A, 1B, S1A, and S1B). OCT4, NESTIN, SOX2, and PAX6 staining together with RT-PCR analysis demonstrated that our protocol allowed for rapid and complete downregulation of rESC pluripotency-related genes, with simultaneous induction of NESC-specific genes (Figures 1C, 1D, and S1C–S1E). After pdD6, NBs were cultured on laminin-coated plates in NESC media containing bFGF, LIF, CHIR99021, and SB431542. After 2 to 3 days, typical two-layer neuroectoderm structures were formed (Figure 1E), which were subjected to dissociation and re-plating/passaging. Upon re-plating, polarized structures started to appear at day 2–3 and later on transformed into polarized miniature NT-like structures (Figures 1F and 1G), which can be further passaged for at least 50 passages.

These NT-like structures uniformly expressed SOX2, SOX1, NESTIN, and PAX6 and clustered ZO-1 and N-CADHERIN, marking the luminal side (Figures 1H–1M). Using phospho-VIMENTIN to label meta-phase cells, we found most (> 90%, 109 in 120 cells) horizontally dividing cells were located on the apical surface (Figure 1N), whereas BrdU-labeled S-phase nuclei were found to be on the basal surface (Figure 1O), indicative of typical interkinetic nuclear migration (IKNM) found in developing NTs in vivo (Willardsen and Link, 2011). These NESCs were negative for GFAP and GLAST (Figure 1P), two RGPC markers, or TBR2 (Figure S1F), a transcriptional factor expressed by outer or inner sub-ventricular-zone RGPCs and intermediate or basal progenitors in the developing primate cortex (Hansen et al., 2010). Taken together, our novel chemically defined neural induction media and the differentiation protocol allow for rapid and robust conversion of rESCs to self-renewing NESCs and, subsequently, miniature NT-like structures.

### Large-Scale Expansion and Stable Conversion of NESCs to Miniature NTs

To our surprise, NESCs in miniature NTs display stable properties as follows. First, rosette or NT structures could be maintained at low or high cell density over passages up to P50 (Figures S1G and S1H). Second, NESCs were routinely passaged at 1:8 to 1:16 every 3 to 4 days, displaying exponential growth over serial passages and resulting in a $2 \times 10^9$-fold increase within 2 months without losing obvious proliferative capacity (Figure S1I). Third, NESCs uniformly express stem cell markers after extensive passaging as indicated by fluorescence-activated cell sorting (FCAS) and immunocytochemical analyses (Figures 1Q and S1J–S1L). Cell-cycle profiles of serial-passaged cells are also stable (Figure S1M). Fourth, NESCs could be frozen and thawed without detectable alterations in proliferation or differentiation and retained a stable karyotype for at least 96 population doublings (P33) (Figure S1N).

### Single NESCs Self-Organize into NT Structures and Undergo Stable Expansion

Given that NESCs in the miniature NTs appear to be highly active, we explored whether single NESCs can undergo serial clonal expansion to self-organize into NTs (Figure 2A). One day after seeding, single NESCs (Figure 2B) exhibited stable proliferation with a highly homogeneous morphology (Figure S3). Progressively, 11.8% and 45.46% of the survival colonies began to organize into rosette forms at days 8 to 10, respectively; 69.7% of the survival colonies eventually self-organized NTs with a lumen-expressing PAX6, NESTIN, ZO-1, and N-CADHERIN at day 14 (Figures 2C–2H and S2). Three-dimensional reconstruction confirmed NT miniature structures being composed of multiple layers of neuroepithelial cells (Movie S1). These single-cell-derived NT cells maintained strong proliferation abilities (Figure 2I). Live imaging of GFP-labeled NESCs showed cells displaying IKNM (Willardsen and Link, 2011) and predominantly horizontal (close to apical side) division (Konno et al., 2008) in NTs (Figure 2J; Movie S2). The efficiency of survival cells and polarized colony (NTs) progressively increased over passages (Figure 2K). The single-cell-derived NT colonies maintained long-term self-renewal and formed stable cell lines. Moreover, 63.13% ± 6.5% of clonal cell-line-derived single cells survived and generated secondary colonies, in which 86.09% ± 7.51% of the survival colonies self-organized into NTs at day 14 following seeding (Figure 2L). Our system allows for repetitive and consistent NT morphogenesis from single cells.

### NESCs Stably Produced Highly Enriched Neurons

NESCs in vivo have strong abilities to differentiate into neurons without astrocytes (Kriegstein and Alvarez-Buylla, 2009). As expected, over serial passaging, NESCs retained a stable propensity toward neuronal differentiation, whereby more than 80% of differentiated cells become

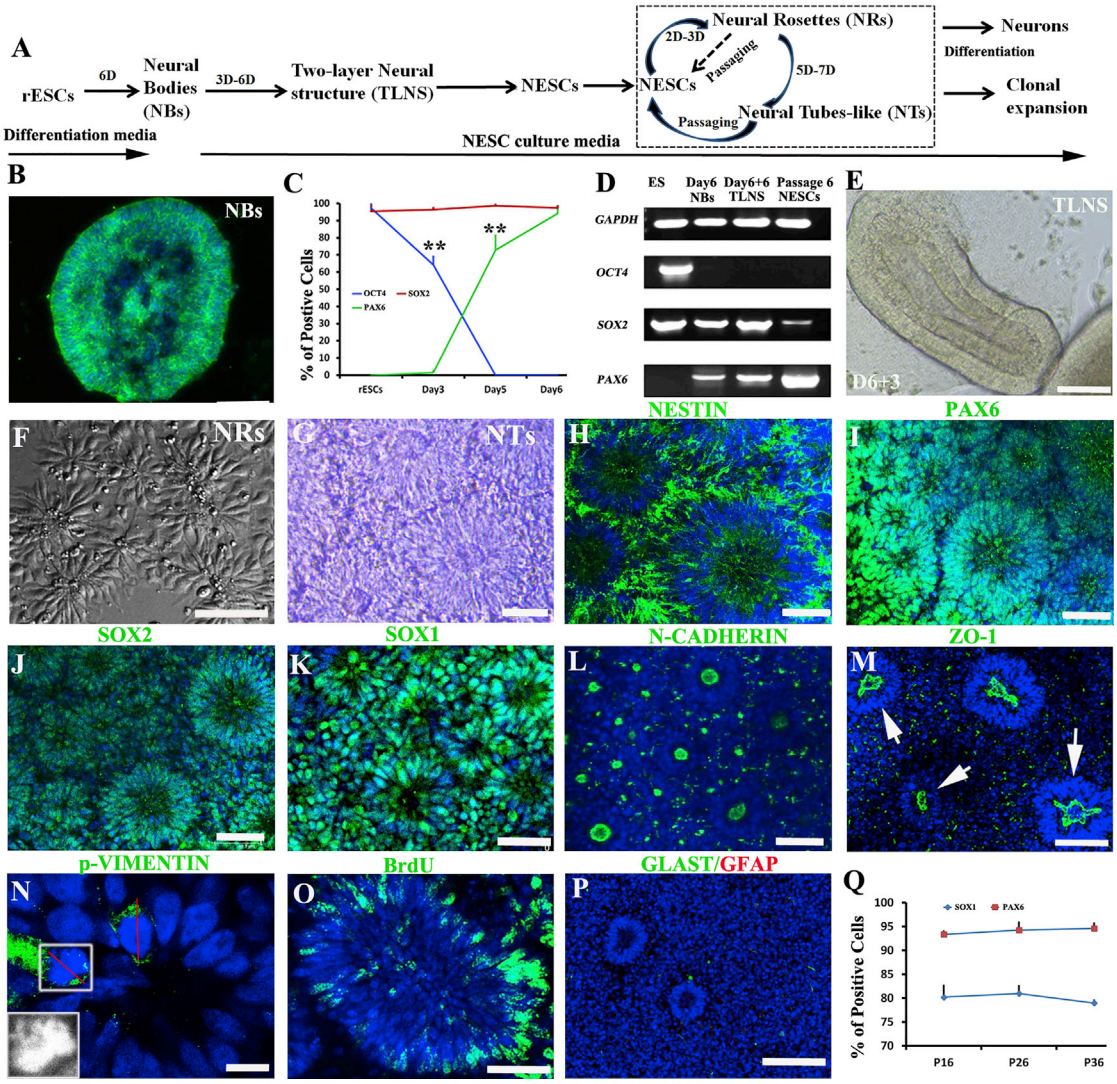


**Figure 1. Rhesus Monkey ESCs Are Rapidly Induced into NESCs**

Three independent experiments were repeated for each line (IVF3.2 and IVF3.3).

(A) Schematic representation of the NESC induction and maintenance process.

(B) Embryonic bodies (EBs) were organized into a neuroepithelial layer structure at post-differentiation day 6 (pdD6) by NESTIN staining.

(C) Quantification of SOX2-, OCT4-, and PAX6-positive cells on pdD2, pdD5, and pdD6. Data are expressed as mean ± SD (data from three independent experiments). **$p < 0.01$ by Student's t test.

(D) RT-PCR of differentiated NBs (pdD6 and pdD12) and expandable NESCs (P6).

(E) NBs at pdD6 attached and formed a two-layer structure after being cultured onto laminin-coated plates for 3 additional days in NESC media.

(F) Representative polarized structures of NESCs at low cell density.

(G) Representative NT structures of NESCs at high cell density.

(H–M) Cultured NESCs maintain NT structures expressing NESC markers NESTIN (H), PAX6 (I), SOX2 (J), SOX1 (K), N-CADHERIN (L), and ZO-1 (M).

(N) Mitotic division marker phospho-VIMENTIN staining. The red line indicates symmetrical horizontal division orientation.

(O) BrdU labeling the S-phase cells in an NT.

(P) NESCs were negative for the radial glial progenitor cell markers GFAP and GLAST.

(Q) Quantification of $SOX1^+$ and $PAX6^+$ cells in serial-passaged NESCs.

Data are expressed as mean ± SD (data from three independent experiments). $p > 0.05$ by Student's t test. Scale bars: (A and B), 200 μm; (J), 100 μm; (N), 10 μm; others, 50 μm.

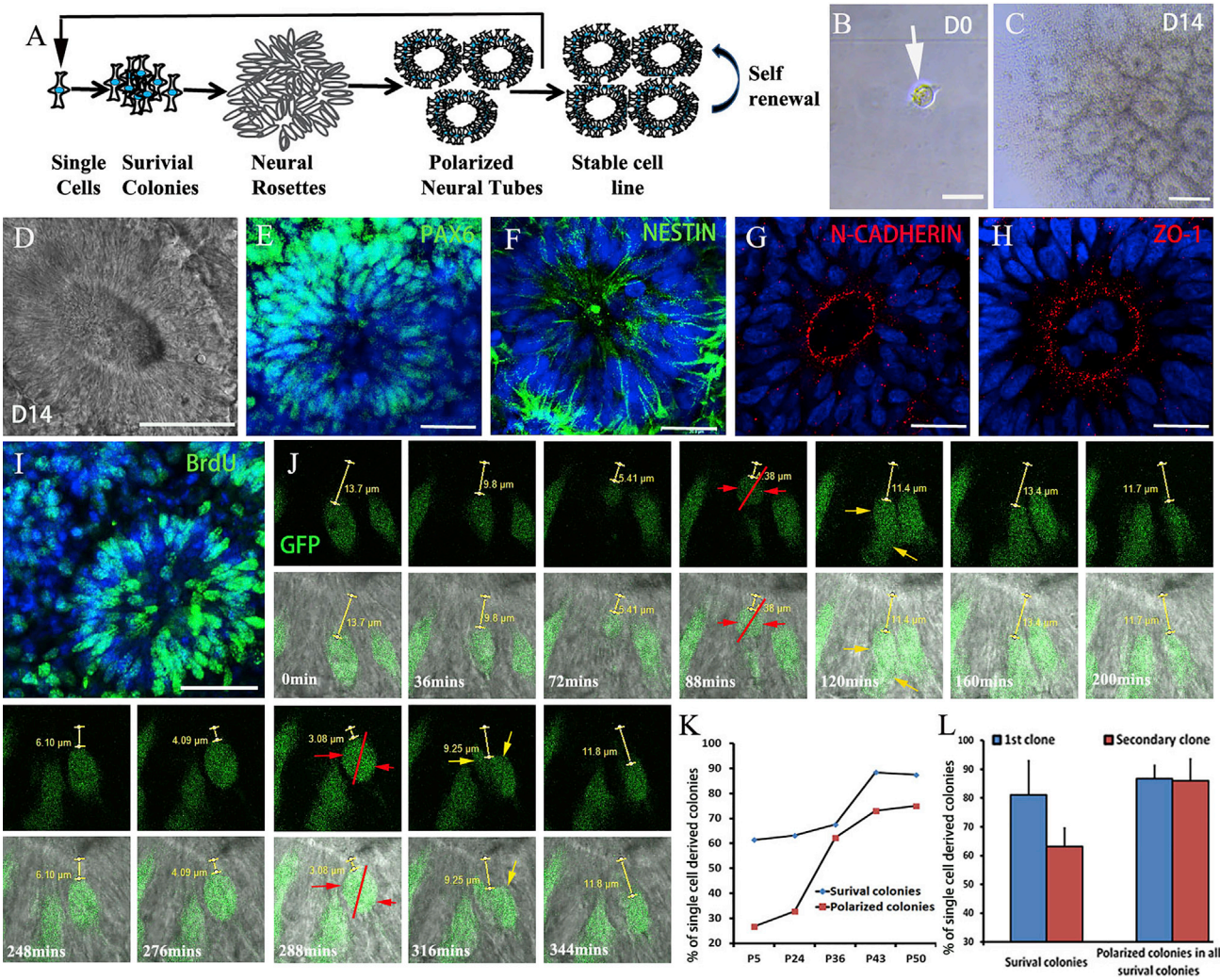


**Figure 2. Single NESCs Self-Organize into Miniature NT-like Structures**

Three independent experiments were repeated for NESCs from IVF3.2 and IVF3.3.

(A) Schematic representation of single-NESC self-organization into NT structures in the continual colony assays.

(B) A NESC on one well of 96-well plate at day 1.

(C and D) Representative one-cell-derived NT structure at day 14.

(E–H) Single-cell-derived NTs expressed NESC markers PAX6 (E), NESTIN (F), N-CADHERIN (G), and ZO-1 (H).

(I) BrdU incorporation of single-cell-derived NTs.

(J) Live imaging of NESC interkinetic nuclear migration in an NT (also see Movie S2). NESC division predominantly displayed horizontal (close to apical surface) orientation. Red arrows indicate two dividing cells; red lines indicate dividing axis; yellow arrows indicate two divided cells; yellow scales indicate the distance between a lumen and $GFP^+$ cells.

(K) Percentages of single-seeded cells on day 14 that formed NESC-derived survival colonies and NT colonies at sequential passages.

(L) Percentage of inoculated single cells that formed survival colonies (phase 1) and the percentage of survival colonies that formed NT colonies (phase 2) during the continual colony assays.

Data are shown as mean ± SD (data from three independent experiments). No significant difference was found ($p > 0.05$). Scale bars: (C and I), 100 μm; others, 20 μm.

neurons without producing astrocytes (Figures 3A and 3B). Interestingly, the proportion of glutamergic to GABAergic neurons in differentiated neurons is closely associated with the cell density. At high density ($9.5 \times 10^3$ cells/$cm^2$), over 99% of differentiated neurons are glutamergic with a few (<1%) being GABAergic (Figures 3C and 3D). In contrast, with low density ($2.1 \times 10^3$ cells/$cm^2$), NESCs-derived GABAergic neurons significantly increased

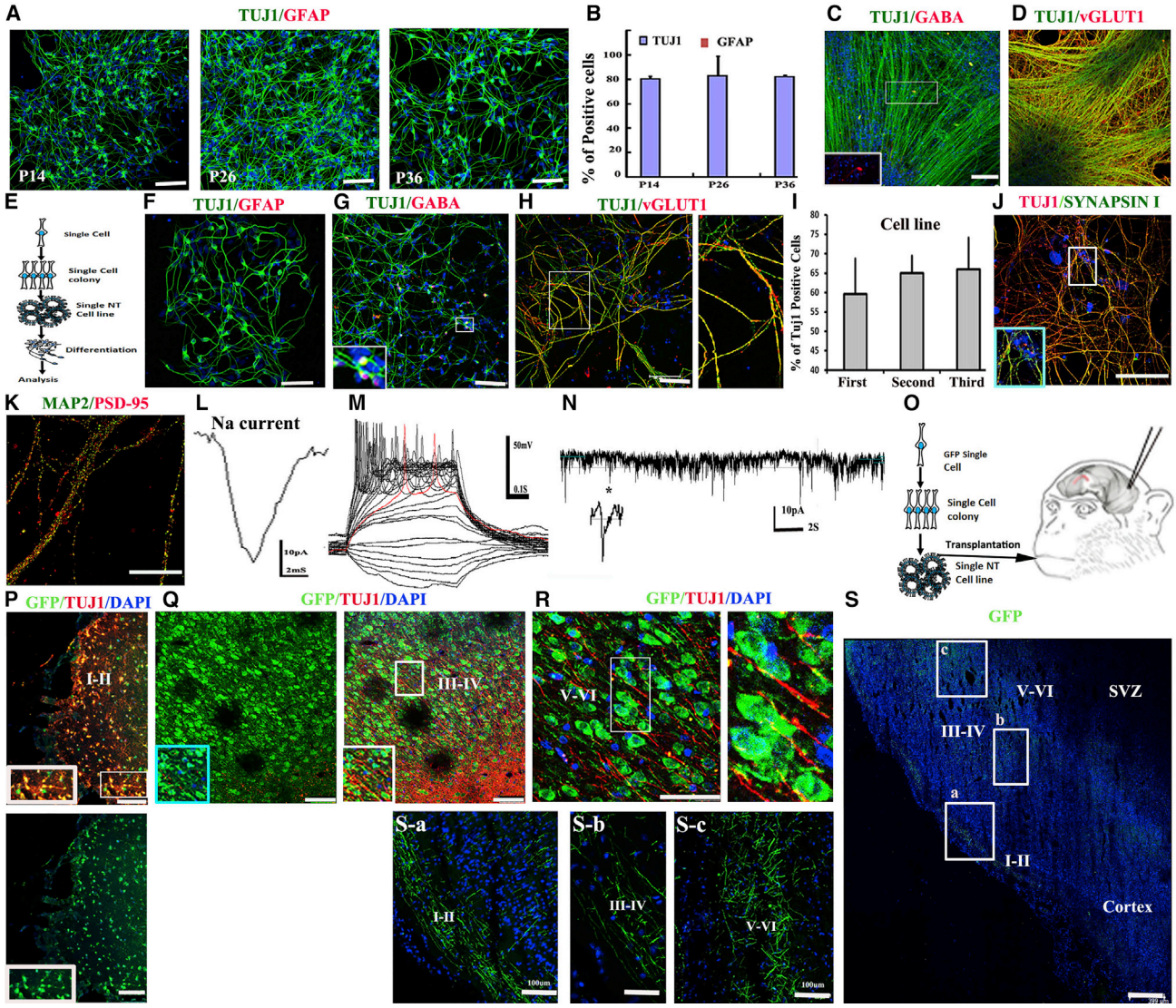


**Figure 3. Single NESCs Produced Functional Neurons and Integrate into Newborn Monkey Brains**

(A and B) Quantification of differentiated Tuj1$^+$ neurons and GFAP$^+$ astrocytes. Data are represented as mean ± SD (data from three independent experiments) ($p > 0.05$ by t test).

(C and D) NESCs differentiated into glutamergic (D) and GABAergic (C) neurons at high cell density.

(E–N) Single-NESC-derived stable cell line gave rise to functional neurons. (E) Schematic representation of single NESC function test assays. (F) Single-NESC-derived progenies differentiated into neurons, but not astrocytes. (G and H) Single-NESC-derived progenies differentiated into glutamergic (H) and GABAergic (G) neurons at low cell density. (I) Quantification of differentiated neurons from three different single-cell-derived progenies. Data are shown as mean ± SD (data from three independent experiments). $p > 0.05$ by t test. (J and K) NESC-derived neurons expressed Synapsin I protein and the post-synapse marker PSD-95 with a punctate pattern. (L and M) A mature neuron exhibited sodium currents and action potentials following current injections. (N) A mature neuron exhibited EPSC.

(O) Schematic representation of single-NESC-derived NT cell transplantation into newborn monkey visual cortex.

(P–R) The injected cells integrated into outer layer (layer I–II) (P), layer III–IV (Q), and layer V–VI (R) of visual cortex and differentiated into neurons.

(S) Injected cells extensively regenerated axon outgrowths, which were found to distribute in the outer layer (I–II) (Sa), deeper layer III–VI (Sb), and layer V–VI (Sc) of cortex.

Scale bars: (K), 50 μm; (S), 400 μm; others, 100 μm.

up to 20.09% ± 7.01%. These data suggest that cell-cell communication plays an important role in NESC neuronal differentiation propensity.

### Individual NESCs Gave Rise to Functional Neurons and Integrated into Newborn Monkey Brains

Differentiation of single-NESC-derived NT cells was spontaneously induced at low cell density to produce functional neurons (Figure 3E). As expected, single NESCs gave rise to glutamergic (76% ± 5.18%) and GABAergic (23.21% ± 3.84%) neurons, not astrocytes (Figures 3F–3H). Quantification of three different single-cell-derived lines showed that they exhibited similar pattern of neuron differentiation (Figure 3I), suggestive of the homogeneity among single NESCs. Furthermore, more than 90% of differentiated neurons were found to form synapse structures expressing Synapsin I pre-synaptic or PSD-95 post-synaptic protein in their axons in a punctate pattern after 32 days or 45 days, respectively, of co-culture with astrocytes (Figures 3J and 3K). Patch clamp recording showed 10 out of the 12 recorded neurons exhibited Na current (Figure 3L) and robust action potential following the current injection (Figure 3M). The recording of functional synapses showed 8 out of the 12 recorded neurons displayed post-synaptic currents (Figure 3N).

To probe the ability of integration into monkey brains for neural repair, single-NESC-derived NT cells labeled by EGFP were injected into the gray matter of visual cortex of two newborn cynomolgus monkeys (postnatal days 24–32) (Figure 3O). After 3 months, the brains were analyzed, and the injected cells were detected on the outermost layer (layer I) (Figure 3P), layer II–III (Figure 3Q), and layer V–IV (Figure 3R) of visual cortex. These cells differentiated into $Tuj1^+$ neurons with typical neuron morphologies (Figures 3P–3R); furthermore, extensive axon outgrowths were found in many sites of cortex and extended from layer I–II into deeper layer of cortex (layer III–VI) (Figures 3Sa–3Sc). Taken together, these data demonstrate that single NESCs behaving as in vivo neuroepithelial cells can produce mature and functional neurons in vitro and in vivo.

### NTs Can Be Generated from Monkey iPSC-Derived NESCs in a Similar Manner

To determine whether monkey induced pluripotent stem cells (iPSCs) could also be induced into NESCs in a similar manner and to build the "NESC-TO-NTs" model, one monkey iPSC line was used, and the experiments described above were repeated. As shown in Figure S3, iPSC-derived NESCs were similarly generated, self-organized into NTs, and maintained stable homogeneous, clonogenic, and neurogenic abilities in culture.

### NESCs Display Unique Metabolism and Active Wnt Signaling Pathways

To test whether NESCs have unique gene expression profiles, the global transcriptome of monkey NESCs at various passages (P5, P24, and P36) were analyzed via RNA sequencing (RNA-seq). P36 RGPCs, only cultured for 7 days in NESC culture media removing CHIR99021 (Figures S4A–S4M), and P36 newly differentiated neurons (NESCs-DN) were also analyzed. Sample correlation (Spearman) showed that late-passage NESCs (P36) closely clustered with mid-passage (P24) and early-passage NESCs (P5) than with RGPCs and NESCs-DN (Figure 4A). Total expression genes were clustered using K means, yielding distinct modules (e.g., modules brown, blue, red, and green) (Figure 4B). Using module Eigengene (Langfelder and Horvath, 2008) or module average gene expression levels, we established correlation between modules and cell types. Several cell-type-specific modules were identified (Figure 4B). For example, the brown module is highly specific for NESCs regardless of passage number, whereas genes in the blue module either are not expressed or are expressed at very low levels in NESCs. On the other hand, the red module appears to be neuronal-specific.

The cell-type-specific modules were subjected to Gene Ontology (GO) analyses (Figures 4C and S5). As expected, GO term enrichment showed NESCs have higher expression of genes related to RNA splicing, energy metabolism, mitochondrion, and purine and pyrimidine metabolism (Figures 4C and S5A). Hub gene analyses of the brown (NESC-specific) module revealed highly connected genes and further confirmed important roles of splicing, mitochondria function, and purine and pyrimidine metabolism for NESCs (Figure 4D). In contrast, neurons express genes relative to axon guidance, neurotrophin signaling pathways, and endocytosis (Figure S5B). In addition, *ASNS*, *LYAR*, and *ZNRF3*, which are hub genes in the brown module (Figure 4D), have recently been shown to be related to microcephaly or NTDs (Hao et al., 2012; Ruzzo et al., 2013; Wang et al., 2012), consistent with the notion that these three factors control NESC development. Moreover, other hub genes such as *LEF1* and *ZNRF3* (Hao et al., 2012) are critical components of the Wnt signaling pathway. Their presence in the brown module hub-gene network suggests that Wnt signaling is involved in regulating NESC biology, consistent with the result from CHIR99021 dropout experiments (Figures 5 and S4).

To identify genes unique to NESCs, RGPCs cultured for only 7 days in media without CHIR99021 were chosen as control to narrow down the candidate gene list. These RGPCs represented newly formed RGPCs as they just began to express GFAP and GLAST but still could be converted back into NESCs upon addition of CHIR99021 (Figures S4A–S4K). Therefore, the transcriptome of these RGPCs is

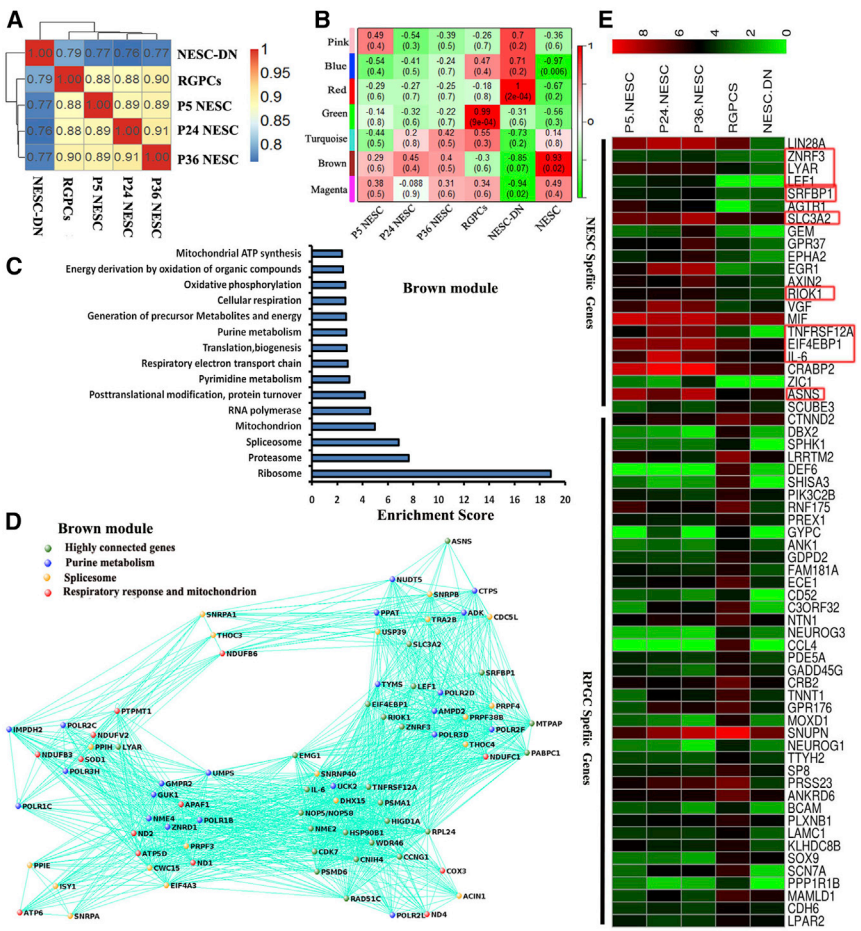


**Figure 4. NESCs Display Unique Metabolism and Active Wnt Signaling Pathways**

(A) Sample correlation (Spearman) of RNA sequencing analysis of the early-, medial-, late-passage NESCs (P5, P24, and P36), RGPCs, and NESCs-ND (differentiated neurons).

(B) K-mean clustering detected modules' relative expression.

(C) Representative GO function terms of NESCs specific to the brown module.

(D) Brown module (NESC-specific) hub-gene network.

(E) Some specific genes expressed at higher levels in NESCs or RGPCs, respectively. Red boxes represent these genes that appeared in the brown module hub-gene network in (D).

only slightly different from that of NESCs (Figure 4A). NESCs uniquely expressed some genes that have been demonstrated to be involved in NT development, such as Wnt signaling genes *LEF1*, *ZIC1* (Merzdorf and Sive, 2006), and *AXIN2* (Bowman et al., 2013), and other NT development genes: *LIN28A* (Balzer et al., 2010), *IL-6* (Islam et al., 2009), and *ASNS* (Ruzzo et al., 2013) (Figure 4E). These data indicate these genes may play critical roles in NESC maintenance.

## NESCs Are Regionally Restricted to a Telencephalic Fate

To further understand whether NESCs are regionally specified by their pattern of gene expression, we used a list of region-specific genes from a published database (Batista-Brito et al., 2008; Elkabetz et al., 2008; Long et al., 2009; Mariani et al., 2012; Zhang et al., 2013). On the basis of the expression levels of these genes, we concluded that the overall expression pattern of the NESCs at different passages (P5, P24, and P36) was typical of forebrain dorsal and ventral features, but not with midbrain, hindbrain, or neural crest features (Figure S6A).

Differentiation assays showed that NESCs gave rise to telencephalic neurons, including dorsal-I-layer to dorsal-VI-layer cortical glutamatergic neurons and ventral GABAergic neurons, but not other neuron subtypes containing N-methyl-D-aspartate receptor (NMDA), adrenergic or serotonergic neurons, and midbrain dopamine and hindbrain neurons (Figure S6B). The differentiation potentials of cortical neurons for NESCs were next evaluated. NESCs underwent $TBR2^{+}PAX6^{-}$ intermediate progenitors and gave rise to $TBR1^{+}$ cortical neurons in SDM media (Figures S6C and S6D). Further characterizations showed that these cortical neurons at least included $BRN2^{+}$ and $CALRETININ^{+}GABA^{-}$ upper-layer neurons as well as $CTIP2^{+}$ and $FOXP2^{+}$ deep-layer neurons (Figures S6E–S6H). In contrast, NESCs were unable to differentiate into adrenergic, serotonergic, and midbrain dopamine neurons (Figure S6I). Furthermore, NESCs failed to produce dopamine neurons in the dopamine differentiation media (Kriks et al., 2011) or motoneurons in the motoneuron differentiation media (Figure S6J) (Hu and Zhang, 2009). NESCs are regionally restricted to a telencephalic fate and have the ability to give rise to cortical neurons.

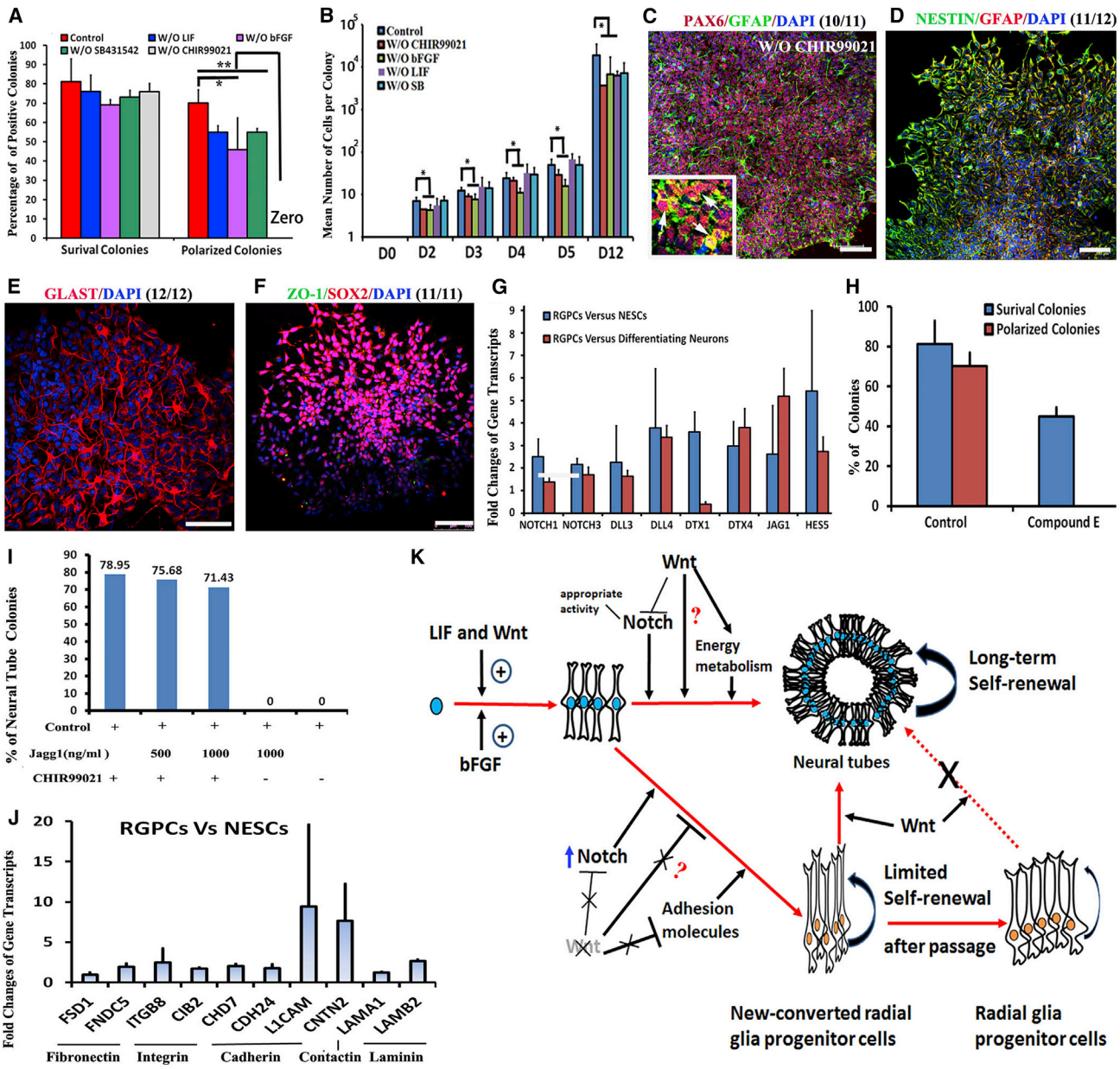


**Figure 5. The Mechanisms Controlling "NESC-TO-NTs" Self-Organization and Radial Glial Progenitor Cell Transition**

(A) Comparison of survival colonies and polarized colonies numbers (as noted by ZO-1 staining) versus the number of seeded single cells on day 14 in five different culture conditions.

(B) The proliferation difference of single cells cultured in five different culture conditions. Data are expressed as mean ± SD (data from three independent experiments) in (A) and (B). *$p < 0.05$; **$p < 0.01$ by Student's t test.

(C–F) Wnt signaling inactivation results in the loss of NT formation and subsequently promotes RGPC transition. Transited cells expressed RGPC markers PAX6 and GFAP (C), NESTIN and GFAP (D), GLAST (E), and SOX2 (F), but not ZO-1 (F).

(G) Fold change of expressions of genes related to Notch signaling in RGPCs versus NESCs and NESCs-DN.

(H) The inhibition of Notch signaling completely abolished NT formation.

(I) Quantification of NT colonies when single NESCs were cultured in different conditions. Jagg1 is a ligand of Notch signaling.

(J) Fold change of expressions of cell adhesion molecules.

(K) Working model of the "NESC-TO-NTs" self-organization and RGPC transition.

Scale bars, 100 μm. Data in (G)–(J) are from three independent experiments.

The NESC identity is different from several published primitive ESC-derived NSCs (Koch et al., 2009a, 2009b) or neural rosette genes (Li et al., 2011), which express a specific set of anterior-posterior neural genes, such as *Hoxb2*, *Nurr1*, *En-1*, *Lmx1b*, *Pax2*, and *Pitx3*, and have the ability to produce midbrain or hindbrain neurons in specific conditions. RNA-seq data further showed NESCs displayed negative or low expression of published neural rosette genes, including *DACH1*, *PLZF*, *LMO3*, *NR2F1*, *DMRT3*, *FLAM70A*, *MMRN1*, and *PLAGL1* as well as *LHX2*, *RFX4*, *ARX*, and *ASCL1*, which are also expressed in FGF2- and EGF-expanded NSCs (Figure S6K) (Elkabetz et al., 2008; Reinhardt et al., 2013), indicating that these genes are unnecessary for maintaining NESCs. Our NESCs with NT formation are different from published neural rosette cells or primitive NSCs.

## Wnt Signaling Was Required for the "NESC-TO-NTs" Self-Organization

To ask whether Wnt signaling is required for the "NESC-TO-NTs" self-organization, the transitions from single NESC to NT structures were analyzed in different culture conditions using dropout experiments. The removal of leukemia inhibitory factor (LIF) alone from the growth media, but not of bFGF or SB431542, resulted in decreased NT formation and secondary NT formation by either decreasing proliferation or promoting differentiation ($p < 0.05$) (Figures 5A and 5B). In contrast, CHIR99021 depletion completely inhibited NT formation (Figures 5A–5E and S4A–S4H). Further studies showed that no stable cell line beyond passage 5 was eventually obtained in the deficient media ($n = 7$), whereas proliferating cell lines were generated from all examined colonies ($n = 3$) in the other three conditions (e.g., without LIF, without SB431542, and without bFGF). These data suggested Wnt signaling is required for the "NESC-TO-NT" conversion.

## Single NESCs Can Undergo RGPC Transition in Absence of Wnt Signaling

To reveal whether NESCs can turn into RGPCs, CHIR99021 alone was removed from NESCs culture media in single-cell cultures. Interestingly, all progenies of single NESCs were progressively converted into $GFAP^+$ cells, which expressed RGPC markers but were no longer capable of NT formation (Figures 5C–5F and S4A–S4H). The early addition of CHIR99021 followed by late withdrawal or early depletion followed by late addition of CHIR99021 showed that GSK3β inhibition was a key to prevent RGPC genesis (Figures S4H–S4K). Although newly formed RGPCs can go back to the NESC state upon CHIR99021 treatment, once passaged, RGPCs lost the ability to convert back to NESCs and differentiate into neurons when LIF, bFGF, and SB431542 were removed from culture media (Figure S4I). Furthermore, addition of XAV939, a Wnt inhibitor, also completely inhibited NT formation and converted NESCs into RGPCs (Figure S4L). These data suggest that Wnt acts to maintain NESC identity via inhibiting transition of RGPCs.

"NESC-TO-RGPC" transition was reported to be regulated by Notch signaling (Gaiano et al., 2000). Interestingly, the genes of Notch signaling are highly expressed in RGPCs compared to in NESCs and NESCs-DN (Figure 5G), which is suggestive of inhibition ability of Wnt signaling to Notch signaling. Elimination of baseline Notch activity, via application of a Notch inhibitor compound E, completely inhibited NT formation (Figure 5H) and promoted neurogenesis (data not shown), whereas the use of a Notch ligand Jagg1 decreased NT formation even in the presence of CHIR99021 (Figure 5I), suggesting that the appropriate level of Notch signaling activity is a key to the delicate balance between NESC maintenance and RGPC transition. However, Jagg1 addition was unable to rescue the NT deficiency caused by CHIR99021 withdrawal (Figure 5I), indicating that Wnt signaling regulated NT formation via regulating other pathways besides Notch signaling. Cell adhesion molecules (CAMs) have been demonstrated to play important roles in neural stem cell (NSC)/NPC self-renewal, differentiation, and neuronal migration (Bian, 2013). Interestingly, we found that expression levels of CAMs, including *Fibronectin*, *Integrin*, *Cadherin*, *L1CAM*, and *CNTN2* (*Contactin-2*), significantly increased during the transition of NESCs to RGPCs (Figure 4J). The working model of Wnt signaling for NT and RPGC transition is summarized in Figure 5K.

## "NESC-TO-NTs" Conversion Could Model NTDs Caused by Folic Acid Deficiency

Despite the strong clinical link between folate and NTDs, the biochemical mechanisms through which folic acid (FA) acts during NT development remain undefined (Momb et al., 2013). To determine whether the "NESC-TO-NTs" conversion in our system has a similar dependence on FA as it does in vivo during NTC, single-cell clonal assays were performed in growth media with and without FA. Mutation or knockouts of a number of key enzymes involved in folate metabolism have been reported to result in NTDs (Figure 6A) (Beaudin et al., 2012; Momb et al., 2013; Padmanabhan et al., 2013). Actually, these key enzymes of folate metabolism were highly expressed in NESCs versus in NESCs-DN or RGPCs (Figure 6B). Furthermore, efficiency of NT formation was closely associated with FA additions (Figure 6C). The increases of FA concentration significantly inhibited NESC apoptosis and promoted NT self-organization when FA concentration was less than 4.5 μM; however, once above 4.5 μM, NESC apoptosis and NT self-organization were negatively correlated with FA concentration. BrdU incorporation showed that NESC proliferation was significantly inhibited in the

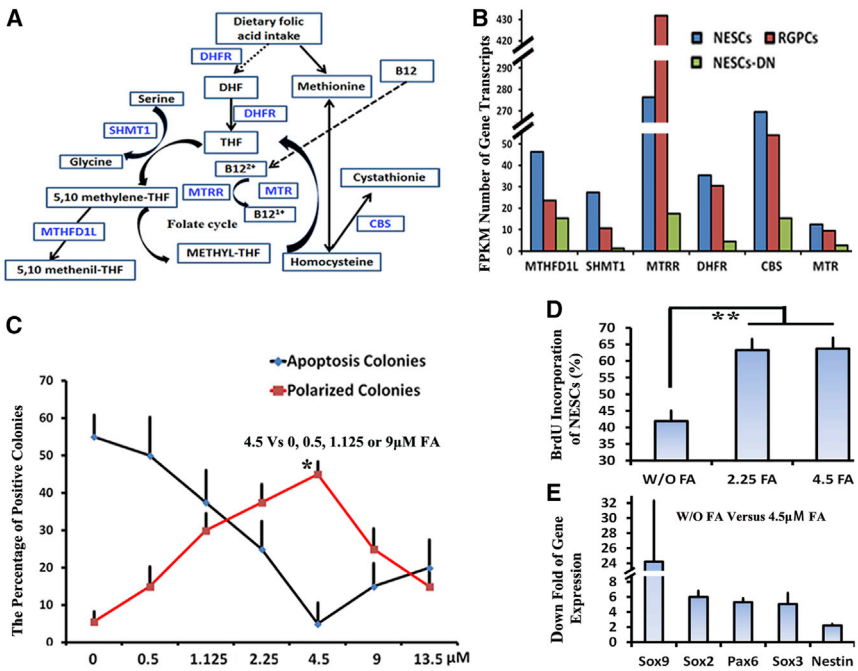


**Figure 6. "NESC-TO-NTs" Conversion Models NTDs Caused by Folic Acid Deficiency**

(A and B) Folate metabolism pathway. Blue names (A) indicate key enzymes involved in folate metabolism whose expression levels are higher in NESCs versus RGPCs or NESCs-DN (B).

(C) NT formation was closely correlated with FA concentrations.

(D) BrdU incorporation assays of NESCs in 2.5 μM FA (2.5FA), 4.5 μM FA (4.5FA), and the media without FA (W/O-NESCs).

(E) Down folds of stem cell markers when NESCs were cultured in the 2.5FA or 4.5FA relative to W/O-NESCs.

Data are showed as mean ± SD in (C), (D), and (E) (data from three independent experiments). *p < 0.05, and **p < 0.01 by Student's t test between each. Data in (B) are from two independent experiments.

absence of FA (Figure 6D). FA deficiency resulted in a significant decrease of stem cell marker expressions (Figure 6E), but not of RPGC and differentiated neuron markers (Figure S7A), indicating that FA deficiency changes stem cell identity not through promoting NESC differentiation. These findings are consistent with previous reports showing that folate deficiency has been established as a risk factor of NTDs (Beaudin et al., 2012; Boyles et al., 2011), whereas FA fortification of the food supply has been temporally associated with declines in the prevalence of NTDs (Botto et al., 2006).

To understand the mechanisms of how FA prevents NTDs, the gene expression profiles from NESCs cultured in media with FA (FA-NESCs) or without FA (W/O-NESCs) were analyzed. Cluster analysis showed that gene expression profiles are significantly different between FA-NESCs and W/O-NESCs (Figure 7A). Differential expression analysis showed that 5,346 genes display significant difference in the two cultures (Table S2). These differential expression genes were clustered using *K* means, yielding four distinct modules (modules turquoise, red, brown, and blue) (Figure 7B). Using module Eigengene (Langfelder and Horvath, 2008) or module average gene expression levels, correlations between modules and cell types were established. Turquoise and red modules are highly or moderately specific for W/O-NESCs, whereas genes in the brown and blue modules are highly or moderately relative to FA-NESCs, respectively. As expected, GO term enrichment of the cell-type-specific modules showed FA presence most significantly promotes expression of genes related to mitosis, cell division, microtubule cytoskeleton, neurogenesis, cell morphogenesis, cell adhesion, neuron migration, and neuron development (Figure 7C; Table S2), which were key for NTC as reported (Copp and Greene, 2013; Copp et al., 2013). Second, FA presence affects expression of genes involved in energy metabolism, chromosome, double-strand break repair, and mitochondrion (Figure S7B; Table S2). In contrast, FA deficiency most significantly induces expression of glycoprotein, the Wnt signaling pathway, growth factor, tube development, and extracellular matrix (Figure 7D; Table S2). FA deprivation affects cell organelles relative to cell death and apoptosis (the Golgi apparatus and endoplasmic reticulum), protein transport, and kinase (Figure S7C; Table S2).

Interestingly, we also noted that FA deficiency significantly inhibited the Wnt signaling activity by upregulating expression of Wnt signaling inhibitors, including *DKK1*, *AXIN2*, and *ZNRF3* (Figure 7E). PCP, Notch, and BMP signaling have been reported to be key for NTC, and their abnormal expressions result in NTDs (Copp and Greene, 2013; Copp et al., 2013). Consistent with these reports, PCP and Notch signaling were significantly downregulated in W/O-NESCs, whereas BMP signaling was upregulated (Figures 7F–7H). We also found that FA maintains normal expression of integrin CAMs, which was involved in NT development (Fournier-Thibault et al., 2009), but not for *CADHERIN*, *LICAM*, and *LAMININ* (Figure 7I). In addition, we found many genes whose expression levels were upregulated for at least 10 folds by FA induction (Figure S7D; Table S2). In contrast, large number of genes, such as *NOTUM*, *DKK1*, *mml-let-7g*, and *IGFBP7*, were specific for

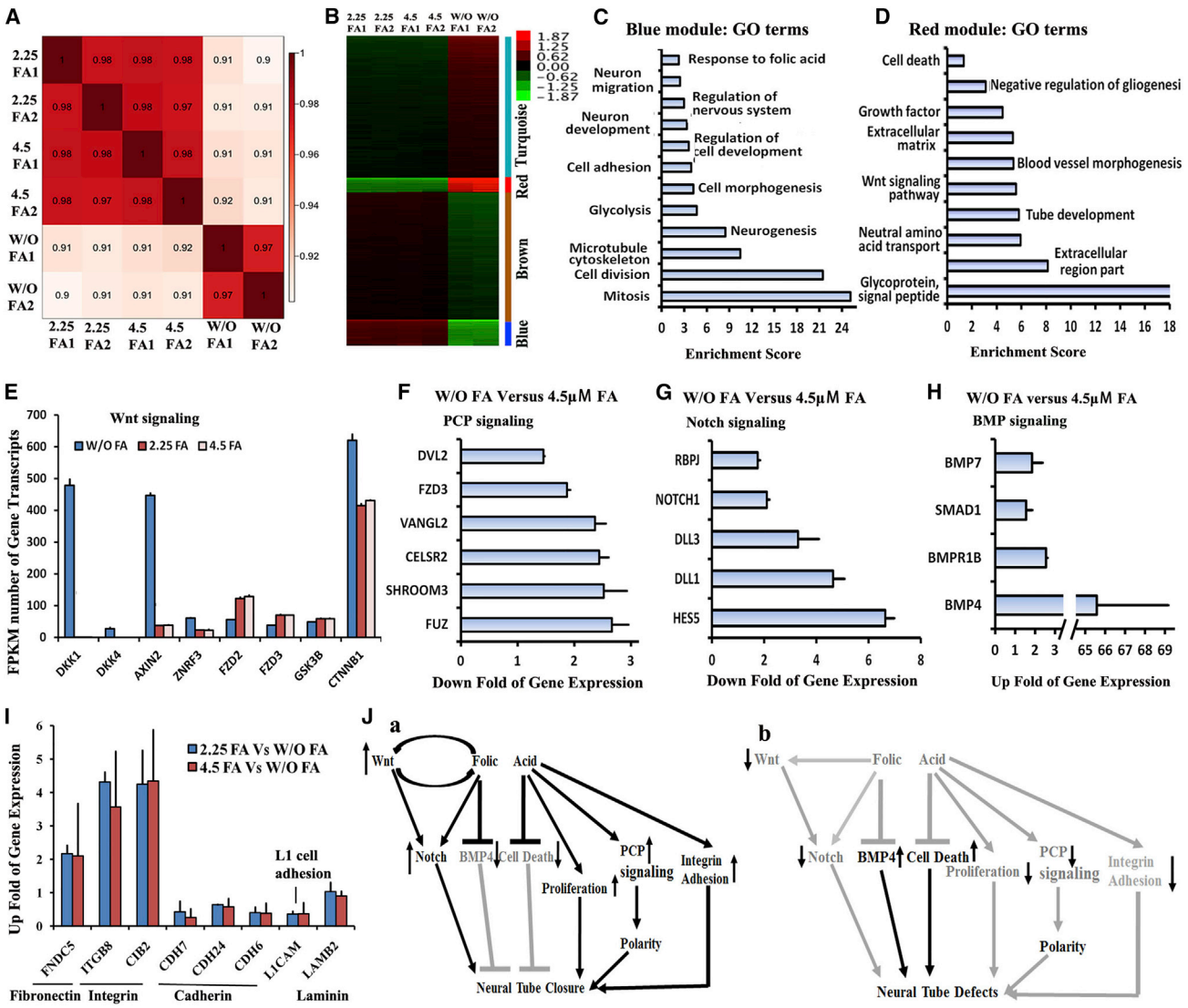


**Figure 7. Folic Acid Can Regulate Multiple Signaling Pathways to Prevent NTDs**

(A) Sample cluster of RNA-seq of NESCs cultured in the without FA media or the 2.25 or 4.5 μM FA media.

(B) K-mean clustering detected modules' relative expression of differential genes between FA-NESCs and W/O-NESCs.

(C) Representative blue-module-specific GO function terms for FA-NESCs.

(D) Representative red-module-specific GO function terms for W/O-NESCs.

(E–I) The change of Wnt signaling (E), PCP signaling (F), and Notch signaling (G) pathways. (H) The change of BMP signaling. (I) The up fold of expression of cell adhesion molecules in FA-NESCs.

(J) The working model of FA inducing NT closure and FA deficiency inducing NTDs.

Data in (E)–(I) are from two independent experiments.

W/O-NESCs, indicating that they are negatively regulated by FA (Figure S7E; Table S2).

Together, these results show that FA promotes NTC by regulating multiple mechanisms, such as activating Wnt, Notch, PCP, and integrin CAM pathways; promoting cell proliferation; and inhibiting BMP4 pathway and cell death (Figure 7J). Thus, the "NESC-TO-NTs" system could recapitulate the FA mechanisms for NTC in vivo and can be used to identify multiple novel candidate genes or pathways involved in NTDs.

## DISCUSSION

In summary, a simple culture system was successfully developed to generate expandable single NESCs derived

from monkey ESCs in vitro. A large number of experiments were used to demonstrate that the system is suitable for studying NTC and related disorders. These cells were found to (1) be polarized neuroepithelial cells; (2) self-organize into miniature NT structures at a cellular level; (3) have robust expansion ability; (4) display IKNM; (5) produce functional neurons and integrate into monkey brains; (6) be dependent on FA for NT formation; (7) express many NT genes, such as *LIN28A*, *ASNS*, *IL-6*, *LYAR*, and *ZNRF3*, but not for RPGC markers, including GFAP, GLAST, and TBR2; and (8) turn into RGPCs once deprived of Wnt signaling. These characteristics show these cells behave similarly as in vivo NT NESCs.

The ability to reproducibly generate NT structures and clonal expansion from single NESCs, as demonstrated in this study, offers several advantages for studying brain development and disease: (1) stability—our NESCs faithfully self-renew. Their cell-cycling parameters, differentiation potentials, gene expression profiles, and NT formation process remain stable for over 50 passes. (2) Single cell function—individual NESCs self-organize into NTs, complete RGPC transition, and give rise to functional neurons. These special properties render the power to reveal how highly complex neural developmental processes organize at a cellular level. (3) Clonal growth—the clonal expansion feature of single NESCs will allow for targeted gene editing facilitated by TALEN (Liu et al., 2014) or CRISPR-Cas9 technologies (Niu et al., 2014). Acquisition of mutant or genetically corrected clones of cells is ideal for disease modeling or mutation corrections using NESCs.

The NT formation and "NESC-to-RGPCs" transition at the onset of neurogenesis are two fundamental events in the early developing brain (Götz and Huttner, 2005). However, the developmental regulations are unclear due to being hard to definitely control the two stages. In this study, the two stages could be definitely regulated at a cellular level. Although Wnt signaling has been demonstrated to play an important role in NSC/NPC formation and function throughout developmental time (Bowman et al., 2013), the effects of Wnt signaling on the two processes are still obscure. Our data clearly showed that both processes are regulated by Wnt signaling activity. Using the system, we found novel insights about the underlying mechanisms of NT formation and RGPC transition. A very interesting discovery is that Notch signaling has an opposite function for the two fates. The specific functions of Notch signaling are related to degree of its activity (Figure 5O). Additionally, previous studies showed L1CAM and CNTN2 are important for neuronal migration, axonal growth, guidance and fasciculation, neuronal survival, and synaptic plasticity (Tonosaki et al., 2014). In the study, L1CAM and CNTN2 were shown to be fundamental to RGPC transition and formation. Thus, the system provides a new platform to study and screen mechanisms of NTC and RGPC transition.

NTDs are severe congenital malformations affecting 1 in every 1,000 pregnancies. Despite the strong clinical link between folate and NTDs, a lack of evidence related to FA pathway mutants and NTD risk pathways indicates the need for novel approaches to elucidate how FA affects NTC. Our present findings show the growth and gene expression characteristics of NESCs are similar to that of NT neuroepithelial cells. Using this system, we demonstrated that FA can regulate multiple mechanisms to prevent NTDs. The relationships among these pathways in NTDs may be uncovered by the system. In addition, we also noted many novel genes regulated by FA. Some novel mechanisms in NTDs might be uncovered by studying their functions. Because of their similarity to humans, NHPs are important models for studying human disease and developing therapeutic strategies. Recently, using TALEN- or CRISPR/Cas9-mediated gene targeting in one-cell embryos, we successfully generated gene mutant rhesus and cynomolgus monkeys (Liu et al., 2014; Niu et al., 2014). If we can identify some key genes for NT development by using the system, using gene editing to produce NTD monkeys with specific genetic mutations will be important to uncover the mechanisms controlling this disorder. Therefore, the system may provide a tractable platform with which to screen small molecules for therapeutic/preventive potential related to NTDs and to help gain new important insights into these disorders.

## EXPERIMENTAL PROCEDURES

### Induction and Expansion of Neuroepithelial Stem Cells

IVF3.2 and IVF3.3 rESCs and monkey fibroblast-derived iPS line 1.1 were cultured on X-ray-inactivated CF-1 mouse embryonic φμbroblasts (MEFs) in ESCs growth media (DMEM/F12 [1:1] [Invitrogen] containing 15% KSR [Invitrogen] and 5 ng/mL bFGF [Millipore]) (Chen et al., 2015; Li et al., 2005; Sun et al., 2011).

ESCs or iPS1.1 were digested with Collagenase IV (Gibco), and neural induction was induced by switching from ESC growth media to differentiation media in suspension culture (Advance DMEM/F12 [1:1] [Invitrogen]: Neurobasal media [Invitrogen] [1:1 mixture] supplemented with 1 × N2 [Invitrogen], 1 × B27 [Invitrogen], 10 ng/ml bFGF [Millipore], 3 μM CHIR99021 [Cellagen Technology], 5 μM SB431542 [Cellagen Technology], 0.2 μM compound E, and 0.1 μM LDN193189 [Cellagen Technology]). After 6 days, EBs were transferred to 5 μg/ml laminin (Gibco)-coated plates for attachment culture, and the media were switched to NESCs culture media (Neurobasal media, including B27, N2, and NEAA [Sigma], 1% Glutmax [Sigma], 3 μM CHIR99021, 5 μM SB431542, 10 ng/ml bFGF, and 1,000 U/ml hLIF [Millipore]). To encourage cell propagation, 0.025% trypsin was used to digest NESCs when passaging. NESCs were routinely passaged to 1:8 to

1:16 ratios every 3 to 4 days. For NT formation, NESCs were continually cultured 8 to 10 days before passaging.

### NESC Differentiation

For spontaneous differentiation, NESCs were cultured on plates coated with laminin (5 μg/ml) and gelatin (0.05%) in differentiation media (SDM) (Neurobasal supplemented with N2, B27, NEAA, and Glutmax). On day 6, 10 ng/ml BDNF (R&D Systems) and 10 ng/ml GDNF (R&D Systems) were added to the media to induce terminal maturation of neurons. For GABAergic neuron differentiation, 10 ng/ml SHH (R&D Systems) was added to the differentiation media for the first 4 days. On day 5, 10 ng/ml BDNF and 10 ng/ml GDNF were added to the media to induce terminal maturation of neurons. For density differentiation experiments, the concentrations of high cell density or low cell density were $9.5 \times 10^3$ cells/cm$^2$ or $2.1 \times 10^3$ cells/cm$^2$, respectively.

### NESCs Modeling Neural Tube Defects Caused by Folic Acid Deficiency

Clonal assays of single NESCs were used as a model to mimic NTDs caused by FA deficiency. After colonies had been cultured in NESC media for 7 days, the media was changed to FA-free NESC media, which constituted RPIM 1640 media, N2, B27, NEAA, 1% Glutmax, 3 μM CHIR99021, 5 μM SB431542, 10 ng/ml bFGF, and 1,000 U/ml hLIF supplemented with different concentrations of FA (Sigma) until day 14. The FA concentrations were 0 μM, 1.125 μM, 2.25 μM, 4.5 μM, 9 μM, and 13.5 μM, respectively. On day 14, apoptosis and NT colonies were quantified as the number of dead colonies or with ZO-1 staining, respectively.

## ACCESSION NUMBERS

The accession number for the RNA sequencing data reported in this paper is GEO: GSE73892.

## SUPPLEMENTAL INFORMATION

Supplemental Information includes Supplemental Experimental Procedures, seven figures, two tables, and two movies and can be found with this article online at http://dx.doi.org/10.1016/j.stemcr.2015.10.007.

## AUTHOR CONTRIBUTIONS

T.L. conceived the idea for this project, designed and conducted experiments, optimized NESCs differentiation and culture conditions, analyzed data, and wrote the manuscript with Y.E.S. and W.J. X.H. and J.R. help to edit the manuscript. X.Z., B.L., Z.A., Z.X., X.Q., Y.C., Y.L., and Y.N. performed experiments and analyzed data under the supervision of T.L. and W.J.; K.Z. analyzed RNA sequencing data.

## ACKNOWLEDGMENTS

This work was funded by grants from the Chinese Ministry of Science and Technology 973 program (2012CBA01307), the Key Technologies Research and Development Program of China (2014BAI03B01), the National Natural Science Foundation of China (31360231 and 31271599), and Yunnan Basic Research Projects (2014FC004).

Received: February 23, 2015
Revised: October 13, 2015
Accepted: October 14, 2015
Published: November 12, 2015

## REFERENCES

Balzer, E., Heine, C., Jiang, Q., Lee, V.M., and Moss, E.G. (2010). LIN28 alters cell fate succession and acts independently of the let-7 microRNA during neurogliogenesis in vitro. Development *137*, 891–900.

Batista-Brito, R., Machold, R., Klein, C., and Fishell, G. (2008). Gene expression in cortical interneuron precursors is prescient of their mature function. Cereb. Cortex *18*, 2306–2317.

Beaudin, A.E., Abarinov, E.V., Malysheva, O., Perry, C.A., Caudill, M., and Stover, P.J. (2012). Dietary folate, but not choline, modifies neural tube defect risk in Shmt1 knockout mice. Am. J. Clin. Nutr. *95*, 109–114.

Bian, S. (2013). Cell adhesion molecules in neural stem cell and stem cell-based therapy for neural disorders. In Neural Stem Cells: New Perspectives, L. Bonfanti, ed. (InTech), pp. 349–380.

Botto, L.D., Lisi, A., Bower, C., Canfield, M.A., Dattani, N., De Vigan, C., De Walle, H., Erickson, D.J., Halliday, J., Irgens, L.M., et al. (2006). Trends of selected malformations in relation to folic acid recommendations and fortification: an international assessment. Birth Defects Res. A Clin. Mol. Teratol. *76*, 693–705.

Bowman, A.N., van Amerongen, R., Palmer, T.D., and Nusse, R. (2013). Lineage tracing with Axin2 reveals distinct developmental and adult populations of Wnt/β-catenin-responsive neural stem cells. Proc. Natl. Acad. Sci. USA *110*, 7324–7329.

Boyles, A.L., Ballard, J.L., Gorman, E.B., McConnaughey, D.R., Cabrera, R.M., Wilcox, A.J., Lie, R.T., and Finnell, R.H. (2011). Association between inhibited binding of folic acid to folate receptor α in maternal serum and folate-related birth defects in Norway. Hum. Reprod. *26*, 2232–2238.

Bush, K.T., Lynch, F.J., DeNittis, A.S., Steinberg, A.B., Lee, H.Y., and Nagele, R.G. (1990). Neural tube formation in the mouse: a morphometric and computerized three-dimensional reconstruction study of the relationship between apical constriction of neuroepithelial cells and the shape of the neuroepithelium. Anat. Embryol. (Berl.) *181*, 49–58.

Chambers, S.M., Fasano, C.A., Papapetrou, E.P., Tomishima, M., Sadelain, M., and Studer, L. (2009). Highly efficient neural conversion of human ES and iPS cells by dual inhibition of SMAD signaling. Nat. Biotechnol. *27*, 275–280.

Chen, Y., Niu, Y., Li, Y., Ai, Z., Kang, Y., Shi, H., Xiang, Z., Yang, Z., Tan, T., Si, W., et al. (2015). Generation of Cynomolgus Monkey Chimeric Fetuses using Embryonic Stem Cells. Cell Stem Cell *17*, 116–124.

Copp, A.J., and Greene, N.D. (2013). Neural tube defects–disorders of neurulation and related embryonic processes. Wiley Interdiscip. Rev. Dev. Biol. *2*, 213–227.

Copp, A.J., Stanier, P., and Greene, N.D.E. (2013). Neural tube defects: recent advances, unsolved questions, and controversies. Lancet Neurol. *12*, 799–810.

Davignon, R.W., Parker, R.M., and Hendrickx, A.G. (1980). Staging of the early embryonic brain in the baboon (Papio cynocephalus) and rhesus monkey (macaca mulatta). Anat. Embryol. (Berl.) *159*, 317–334.

Elkabetz, Y., Panagiotakos, G., Al Shamy, G., Socci, N.D., Tabar, V., and Studer, L. (2008). Human ES cell-derived neural rosettes reveal a functionally distinct early neural stem cell stage. Genes Dev. *22*, 152–165.

Espuny-Camacho, I., Michelsen, K.A., Gall, D., Linaro, D., Hasche, A., Bonnefont, J., Bali, C., Orduz, D., Bilheu, A., Herpoel, A., et al. (2013). Pyramidal neurons derived from human pluripotent stem cells integrate efficiently into mouse brain circuits in vivo. Neuron *77*, 440–456.

Fish, J.L., Kosodo, Y., Enard, W., Pääbo, S., and Huttner, W.B. (2006). Aspm specifically maintains symmetric proliferative divisions of neuroepithelial cells. Proc. Natl. Acad. Sci. USA *103*, 10438–10443.

Fournier-Thibault, C., Blavet, C., Jarov, A., Bajanca, F., Thorsteinsdóttir, S., and Duband, J.L. (2009). Sonic hedgehog regulates integrin activity, cadherin contacts, and cell polarity to orchestrate neural tube morphogenesis. J. Neurosci. *29*, 12506–12520.

Gaiano, N., Nye, J.S., and Fishell, G. (2000). Radial glial identity is promoted by Notch1 signaling in the murine forebrain. Neuron *26*, 395–404.

Götz, M., and Huttner, W.B. (2005). The cell biology of neurogenesis. Nat. Rev. Mol. Cell Biol. *6*, 777–788.

Hansen, D.V., Lui, J.H., Parker, P.R.L., and Kriegstein, A.R. (2010). Neurogenic radial glia in the outer subventricular zone of human neocortex. Nature *464*, 554–561.

Hao, H.-X., Xie, Y., Zhang, Y., Charlat, O., Oster, E., Avello, M., Lei, H., Mickanin, C., Liu, D., Ruffner, H., et al. (2012). ZNRF3 promotes Wnt receptor turnover in an R-spondin-sensitive manner. Nature *485*, 195–200.

Hu, B.-Y., and Zhang, S.-C. (2009). Differentiation of spinal motor neurons from pluripotent human stem cells. Nat. Protoc. *4*, 1295–1304.

Islam, O., Gong, X., Rose-John, S., and Heese, K. (2009). Interleukin-6 and neural stem cells: more than gliogenesis. Mol. Biol. Cell *20*, 188–199.

Koch, P., Opitz, T., Steinbeck, J.A., Ladewig, J., and Brüstle, O. (2009a). A rosette-type, self-renewing human ES cell-derived neural stem cell with potential for in vitro instruction and synaptic integration. Proc. Natl. Acad. Sci. USA *106*, 3225–3230.

Konno, D., Shioi, G., Shitamukai, A., Mori, A., Kiyonari, H., Miyata, T., and Matsuzaki, F. (2008). Neuroepithelial progenitors undergo LGN-dependent planar divisions to maintain self-renewability during mammalian neurogenesis. Nat. Cell Biol. *10*, 93–101.

Kriegstein, A.R., and Götz, M. (2003). Radial glia diversity: a matter of cell fate. Glia *43*, 37–43.

Kriegstein, A., and Alvarez-Buylla, A. (2009). The glial nature of embryonic and adult neural stem cells. Annu. Rev. Neurosci. *32*, 149–184.

Kriks, S., Shim, J.-W., Piao, J., Ganat, Y.M., Wakeman, D.R., Xie, Z., Carrillo-Reid, L., Auyeung, G., Antonacci, C., Buch, A., et al. (2011). Dopamine neurons derived from human ES cells efficiently engraft in animal models of Parkinson's disease. Nature *480*, 547–551.

Lancaster, M.A., Renner, M., Martin, C.-A., Wenzel, D., Bicknell, L.S., Hurles, M.E., Homfray, T., Penninger, J.M., Jackson, A.P., and Knoblich, J.A. (2013). Cerebral organoids model human brain development and microcephaly. Nature *501*, 373–379.

Langfelder, P., and Horvath, S. (2008). WGCNA: an R package for weighted correlation network analysis. BMC Bioinformatics *9*, 559.

LaVaute, T.M., Yoo, Y.D., Pankratz, M.T., Weick, J.P., Gerstner, J.R., and Zhang, S.-C. (2009). Regulation of neural specification from human embryonic stem cells by BMP and FGF. Stem Cells *27*, 1741–1749.

Li, T., Wang, S., Xie, Y., Lu, Y., Zhang, X., Wang, L., Yang, S., Wolf, D., Zhou, Q., and Ji, W. (2005). Homologous feeder cells support undifferentiated growth and pluripotency in monkey embryonic stem cells. Stem Cells *23*, 1192–1199.

Li, W., Sun, W., Zhang, Y., Wei, W., Ambasudhan, R., Xia, P., Talantova, M., Lin, T., Kim, J., Wang, X., et al. (2011). Rapid induction and long-term self-renewal of primitive neural precursors from human embryonic stem cells by small molecule inhibitors. Proc. Natl. Acad. Sci. USA *108*, 8299–8304.

Liu, H., Chen, Y., Niu, Y., Zhang, K., Kang, Y., Ge, W., Liu, X., Zhao, E., Wang, C., Lin, S., et al. (2014). TALEN-mediated gene mutagenesis in rhesus and cynomolgus monkeys. Cell Stem Cell *14*, 323–328.

Long, J.E., Cobos, I., Potter, G.B., and Rubenstein, J.L.R. (2009). Dlx1&2 and Mash1 transcription factors control MGE and CGE patterning and differentiation through parallel and overlapping pathways. Cereb. Cortex *19* (*Suppl 1*), i96–i106.

Lyashenko, N., Winter, M., Migliorini, D., Biechele, T., Moon, R.T., and Hartmann, C. (2011). Differential requirement for the dual functions of β-catenin in embryonic stem cell self-renewal and germ layer formation. Nat. Cell Biol. *13*, 753–761.

Mariani, J., Simonini, M.V., Palejev, D., Tomasini, L., Coppola, G., Szekely, A.M., Horvath, T.L., and Vaccarino, F.M. (2012). Modeling human cortical development in vitro using induced pluripotent stem cells. Proc. Natl. Acad. Sci. USA *109*, 12770–12775.

Meinhardt, A., Eberle, D., Tazaki, A., Ranga, A., Niesche, M., Wilsch-Bräuninger, M., Stec, A., Schackert, G., Lutolf, M., and Tanaka, E.M. (2014). 3D reconstitution of the patterned neural tube from embryonic stem cells. Stem Cell Reports *3*, 987–999.

Merzdorf, C.S., and Sive, H.L. (2006). The zic1 gene is an activator of Wnt signaling. Int. J. Dev. Biol. *50*, 611–617.

Momb, J., Lewandowski, J.P., Bryant, J.D., Fitch, R., Surman, D.R., Vokes, S.A., and Appling, D.R. (2013). Deletion of Mthfd1l causes embryonic lethality and neural tube and craniofacial defects in mice. Proc. Natl. Acad. Sci. USA *110*, 549–554.

Niu, Y., Shen, B., Cui, Y., Chen, Y., Wang, J., Wang, L., Kang, Y., Zhao, X., Si, W., Li, W., et al. (2014). Generation of gene-modified cynomolgus monkey via Cas9/RNA-mediated gene targeting in one-cell embryos. Cell *156*, 836–843.

Padmanabhan, N., Jia, D., Geary-Joo, C., Wu, X., Ferguson-Smith, A.C., Fung, E., Bieda, M.C., Snyder, F.F., Gravel, R.A., Cross, J.C., and Watson, E.D. (2013). Mutation in folate metabolism causes epigenetic instability and transgenerational effects on development. Cell *155*, 81–93.

Reinhardt, P., Glatza, M., Hemmer, K., Tsytsyura, Y., Thiel, C.S., Höing, S., Moritz, S., Parga, J.A., Wagner, L., Bruder, J.M., et al. (2013). Derivation and expansion using only small molecules of human neural progenitors for neurodegenerative disease modeling. PLoS ONE *8*, e59252.

Ruzzo, E.K., Capo-Chichi, J.M., Ben-Zeev, B., Chitayat, D., Mao, H., Pappas, A.L., Hitomi, Y., Lu, Y.F., Yao, X., Hamdan, F.F., et al. (2013). Deficiency of asparagine synthetase causes congenital microcephaly and a progressive form of encephalopathy. Neuron *80*, 429–441.

Sun, Z., Wei, Q., Zhang, Y., He, X., Ji, W., and Su, B. (2011). MicroRNA profiling of rhesus macaque embryonic stem cells. BMC Genomics *12*, 276.

Tonosaki, M., Itoh, K., Umekage, M., Kishimoto, T., Yaoi, T., Lemmon, V.P., and Fushiki, S. (2014). L1cam is crucial for cell locomotion and terminal translocation of the Soma in radial migration during murine corticogenesis. PLoS ONE *9*, e86186.

Wallingford, J.B., Niswander, L.A., Shaw, G.M., and Finnell, R.H. (2013). The continuing challenge of understanding, preventing, and treating neural tube defects. Science *339*, 1222002.

Wang, G., Fulkerson, C.M., Malek, R., Ghassemifar, S., Snyder, P.W., and Mendrysa, S.M. (2012). Mutations in Lyar and p53 are synergistically lethal in female mice. Birth Defects Res. A Clin. Mol. Teratol. *94*, 729–737.

Willardsen, M.I., and Link, B.A. (2011). Cell biological regulation of division fate in vertebrate neuroepithelial cells. Dev. Dyn. *240*, 1865–1879.

Zhang, Y., Pak, C., Han, Y., Ahlenius, H., Zhang, Z., Chanda, S., Marro, S., Patzke, C., Acuna, C., Covy, J., et al. (2013). Rapid single-step induction of functional neurons from human pluripotent stem cells. Neuron *78*, 785–798.

**Stem Cell Reports, Volume *6***

## Supplemental Information

# A Robust Single Primate Neuroepithelial Cell Clonal Expansion System for Neural Tube Development and Disease Studies

**Xiaoqing Zhu, Bo Li, Zongyong Ai, Zheng Xiang, Kunshang Zhang, Xiaoyan Qiu, Yongchang Chen, Yuemin Li, Joshua D. Rizak, Yuyu Niu, Xintian Hu, Yi Eve Sun, Weizhi Ji, and Tianqing Li**

**Supplemental Figures**

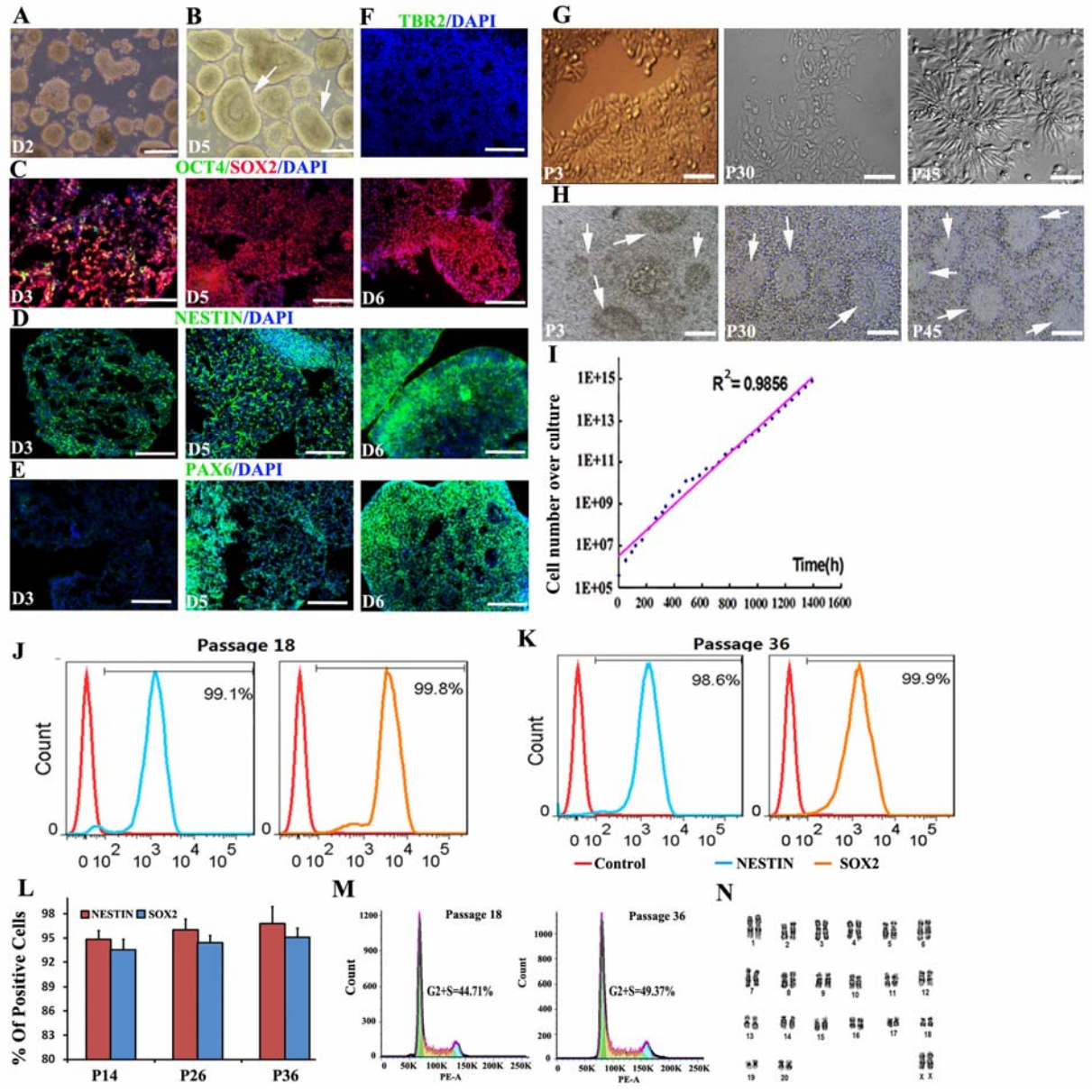


Figure S1.

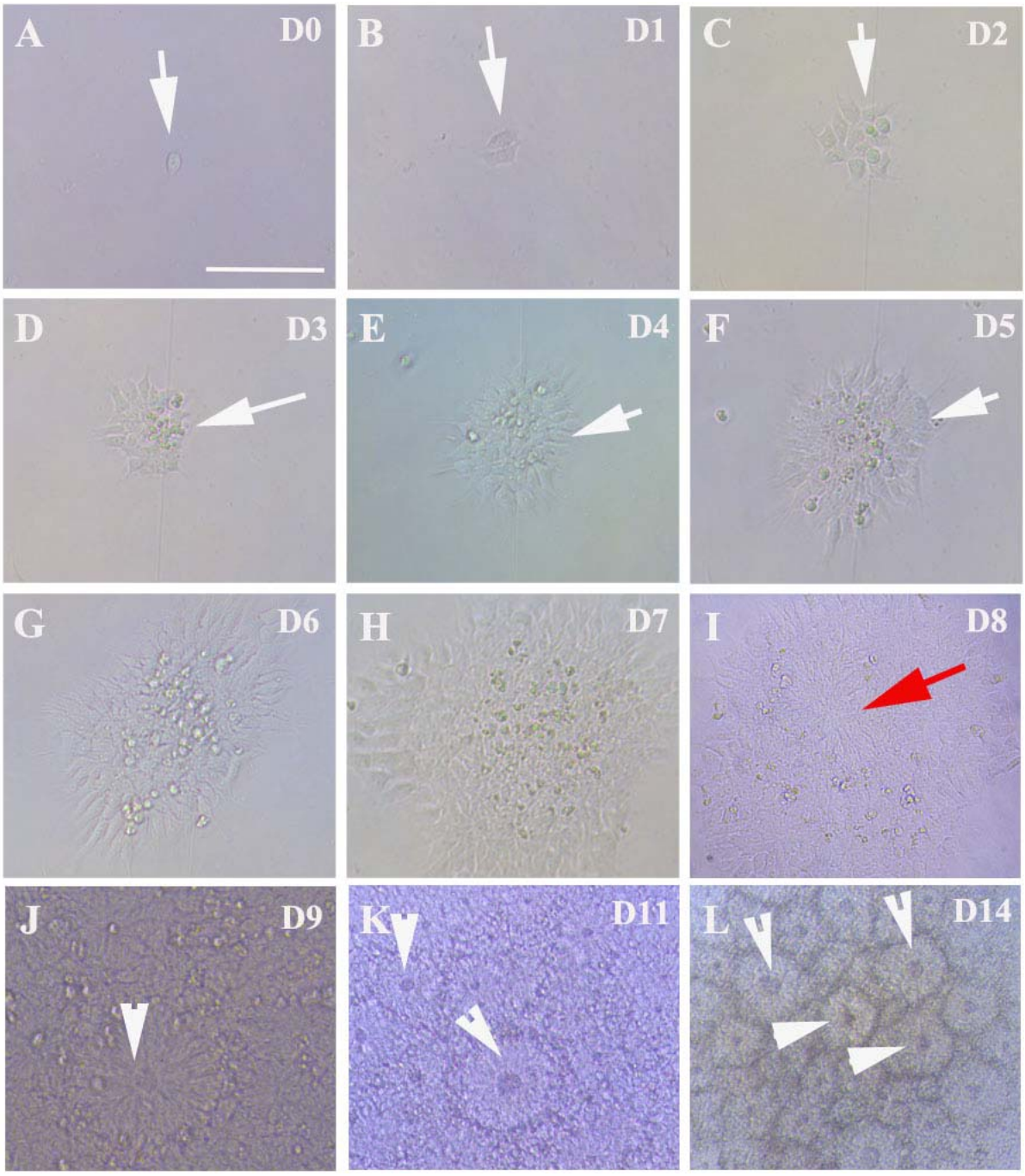


Figure S2

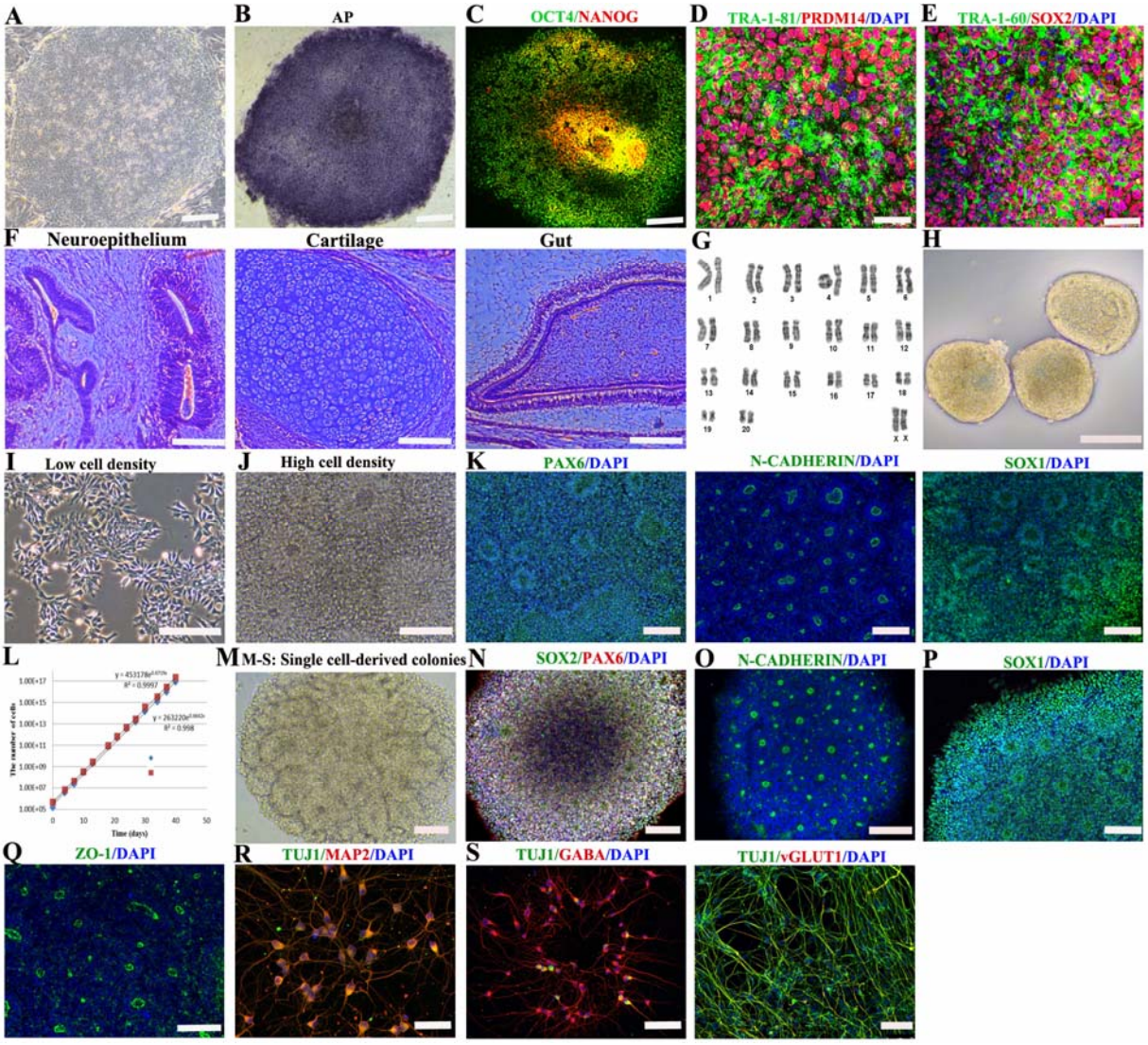
A
B
AP
C
OCT4/NANOG
D
TRA-1-81/PRDM14/DAPI
E
TRA-1-60/SOX2/DAPI
F
Neuroepithelium
Cartilage
Gut
G
H
I
Low cell density
J
High cell density
K
PAX6/DAPI
N-CADHERIN/DAPI
SOX1/DAPI
L
M
M-S: Single cell-derived colonies
N
SOX2/PAX6/DAPI
O
N-CADHERIN/DAPI
P
SOX1/DAPI
Q
ZO-1/DAPI
R
TUJ1/MAP2/DAPI
S
TUJ1/GABA/DAPI
TUJ1/vGLUT1/DAPI

Figure S3

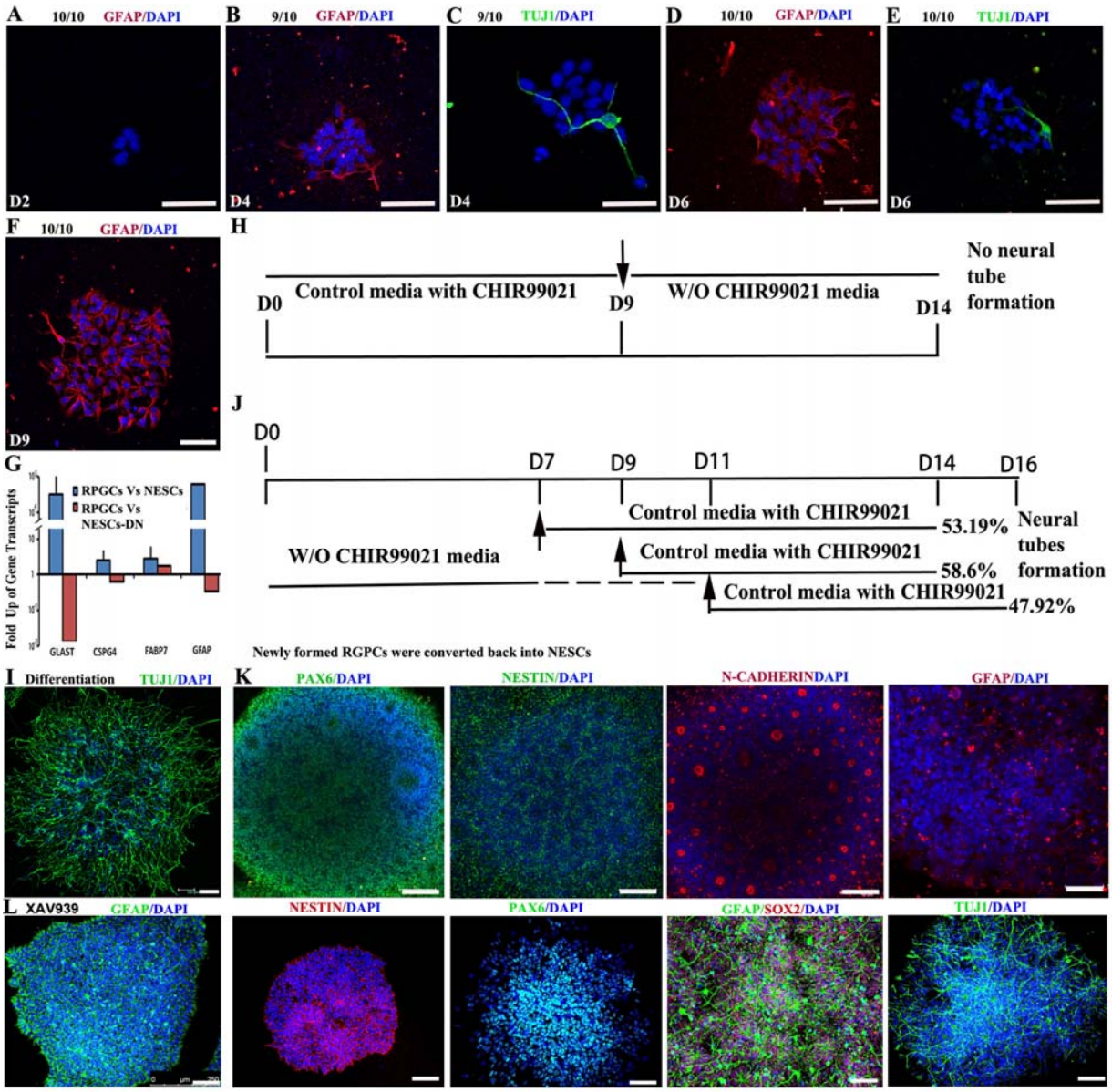
A 10/10 GFAP/DAPI
D2
B 9/10 GFAP/DAPI
D4
C 9/10 TUJ1/DAPI
D4
D 10/10 GFAP/DAPI
D6
E 10/10 TUJ1/DAPI
D6
F 10/10 GFAP/DAPI
D9
H
Control media with CHIR99021
W/O CHIR99021 media
D0
D9
D14
No neural tube formation
J
D0
D7
D9
D11
D14
D16
Control media with CHIR99021
53.19%
W/O CHIR99021 media
Control media with CHIR99021
58.6%
Control media with CHIR99021
47.92%
Neural tubes formation
G
RPGCs Vs NESCs
RPGCs Vs NESCs-DN
Fold Up of Gene Transcripts
GLAST
CSPG4
FABP7
GFAP
Newly formed RGPCs were converted back into NESCs
I Differentiation TUJ1/DAPI
K PAX6/DAPI
NESTIN/DAPI
N-CADHERINDAPI
GFAP/DAPI
L XAV939 GFAP/DAPI
NESTIN/DAPI
PAX6/DAPI
GFAP/SOX2/DAPI
TUJ1/DAPI

Figure S4.

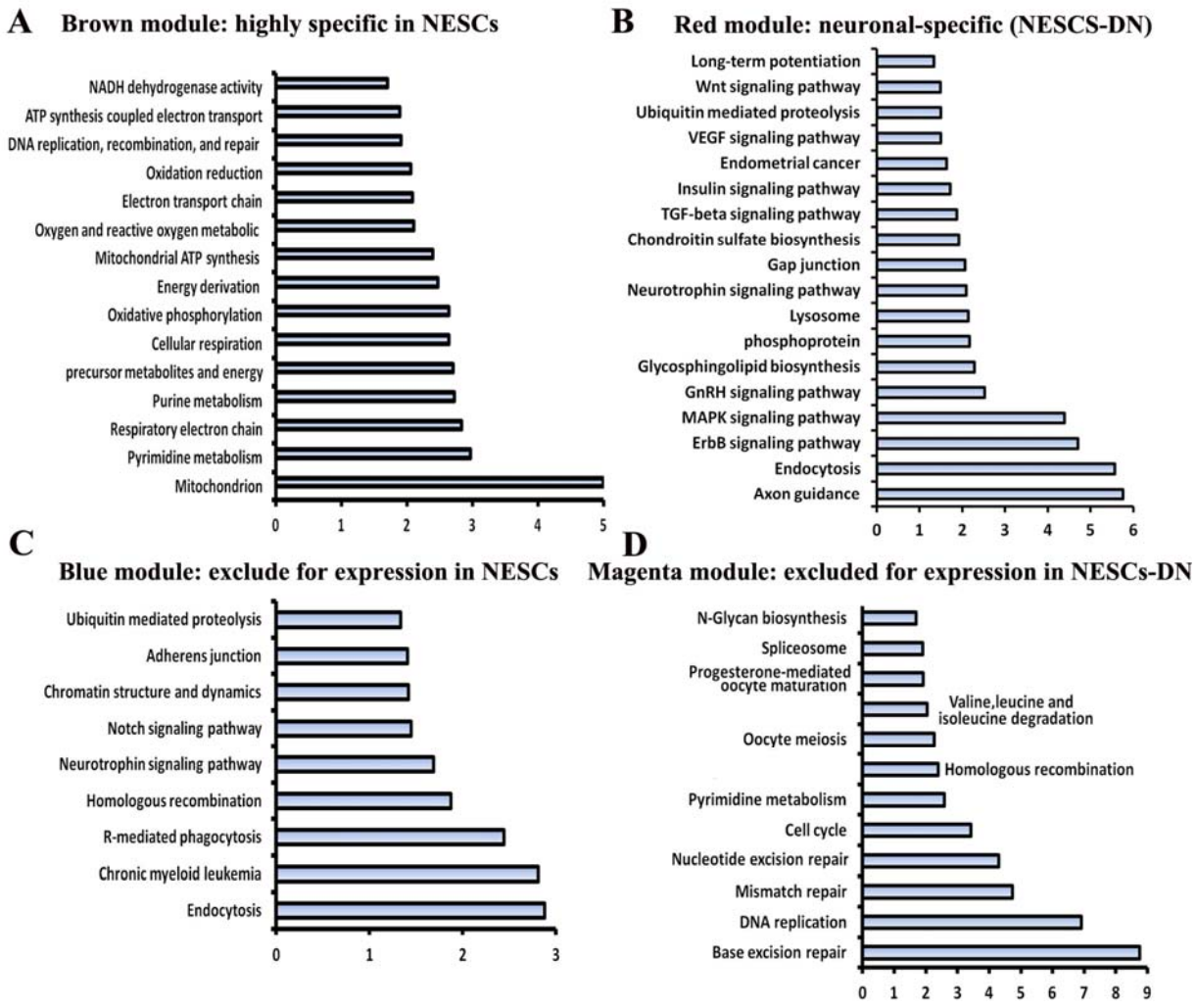
A
Brown module: highly specific in NESCs
NADH dehydrogenase activity
ATP synthesis coupled electron transport
DNA replication, recombination, and repair
Oxidation reduction
Electron transport chain
Oxygen and reactive oxygen metabolic
Mitochondrial ATP synthesis
Energy derivation
Oxidative phosphorylation
Cellular respiration
precursor metabolites and energy
Purine metabolism
Respiratory electron chain
Pyrimidine metabolism
Mitochondrion
0 1 2 3 4 5
B
Red module: neuronal-specific (NESCS-DN)
Long-term potentiation
Wnt signaling pathway
Ubiquitin mediated proteolysis
VEGF signaling pathway
Endometrial cancer
Insulin signaling pathway
TGF-beta signaling pathway
Chondroitin sulfate biosynthesis
Gap junction
Neurotrophin signaling pathway
Lysosome
phosphoprotein
Glycosphingolipid biosynthesis
GnRH signaling pathway
MAPK signaling pathway
ErbB signaling pathway
Endocytosis
Axon guidance
0 1 2 3 4 5 6
C
Blue module: exclude for expression in NESCs
Ubiquitin mediated proteolysis
Adherens junction
Chromatin structure and dynamics
Notch signaling pathway
Neurotrophin signaling pathway
Homologous recombination
R-mediated phagocytosis
Chronic myeloid leukemia
Endocytosis
0 1 2 3
D
Magenta module: excluded for expression in NESCs-DN
N-Glycan biosynthesis
Spliceosome
Progesterone-mediated oocyte maturation
Valine,leucine and isoleucine degradation
Oocyte meiosis
Homologous recombination
Pyrimidine metabolism
Cell cycle
Nucleotide excision repair
Mismatch repair
DNA replication
Base excision repair
0 1 2 3 4 5 6 7 8 9

Figure S5.

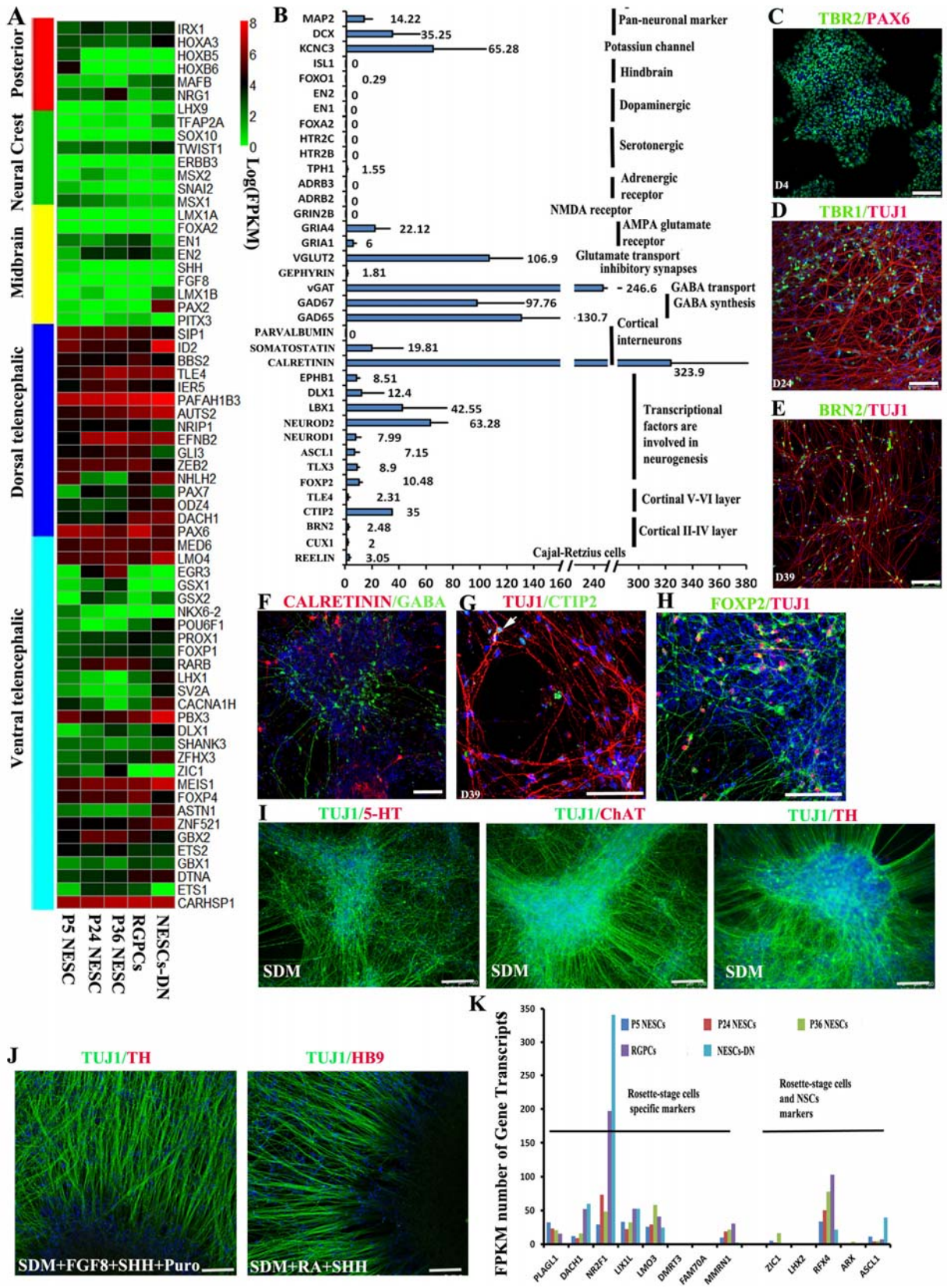
A
Posterior
Neural Crest
Midbrain
Dorsal telencephalic
Ventral telencephalic
IRX1
HOXA3
HOXB5
HOXB6
MAFB
NRG1
LHX9
TFAP2A
SOX10
TWIST1
ERBB3
MSX2
SNAI2
MSX1
LMX1A
FOXA2
EN1
EN2
SHH
FGF8
LMX1B
PAX2
PITX3
SIP1
ID2
BBS2
TLE4
IER5
PAFAH1B3
AUTS2
NRIP1
EFNB2
GLI3
ZEB2
NHLH2
PAX7
ODZ4
DACH1
PAX6
MED6
LMO4
EGR3
GSX1
GSX2
NKX6-2
POU6F1
PROX1
FOXP1
RARB
LHX1
SV2A
CACNA1H
PBX3
DLX1
SHANK3
ZFHX3
ZIC1
MEIS1
FOXP4
ASTN1
ZNF521
GBX2
ETS2
GBX1
DTNA
ETS1
CARHSP1
8
6
4
2
0
Log(FPKM)
P5 NESC
P24 NESC
P36 NESC
RGPCs
NESCs-DN
B
MAP2 14.22
DCX 35.25
KCNC3 65.28
ISL1 0
FOXO1 0.29
EN2 0
EN1 0
FOXA2 0
HTR2C 0
HTR2B 0
TPH1 1.55
ADRB3 0
ADRB2 0
GRIN2B 0
GRIA4 22.12
GRIA1 6
VGLUT2 106.9
GEPHYRIN 1.81
vGAT 246.6
GAD67 97.76
GAD65 130.7
PARVALBUMIN 0
SOMATOSTATIN 19.81
CALRETININ 323.9
EPHB1 8.51
DLX1 12.4
LBX1 42.55
NEUROD2 63.28
NEUROD1 7.99
ASCL1 7.15
TLX3 8.9
FOXP2 10.48
TLE4 2.31
CTIP2 35
BRN2 2.48
CUX1 2
REELIN 3.05
Pan-neuronal marker
Potassiun channel
Hindbrain
Dopaminergic
Serotonergic
Adrenergic receptor
NMDA receptor
AMPA glutamate receptor
Glutamate transport inhibitory synapses
GABA transport
GABA synthesis
Cortical interneurons
Transcriptional factors are involved in neurogenesis
Cortinal V-VI layer
Cortical II-IV layer
Cajal-Retzius cells
0 20 40 60 80 100 120 140 160 240 300 320 340 360 380
C TBR2/PAX6
D4
D TBR1/TUJ1
D24
E BRN2/TUJ1
D39
F CALRETININ/GABA
G TUJ1/CTIP2
D39
H FOXP2/TUJ1
I TUJ1/5-HT
TUJ1/ChAT
TUJ1/TH
SDM
SDM
SDM
J TUJ1/TH
TUJ1/HB9
SDM+FGF8+SHH+Puro
SDM+RA+SHH
K
FPKM number of Gene Transcripts
350
300
250
200
150
100
50
0
P5 NESCs
P24 NESCs
P36 NESCs
RGPCs
NESCs-DN
Rosette-stage cells specific markers
Rosette-stage cells and NSCs markers
PLAGL1
DACH1
NR2F1
LIX1L
LMO3
DMRT3
FAM70A
MMRN1
ZIC1
LHX2
RFX4
ARX
ASCL1

Figure S6.

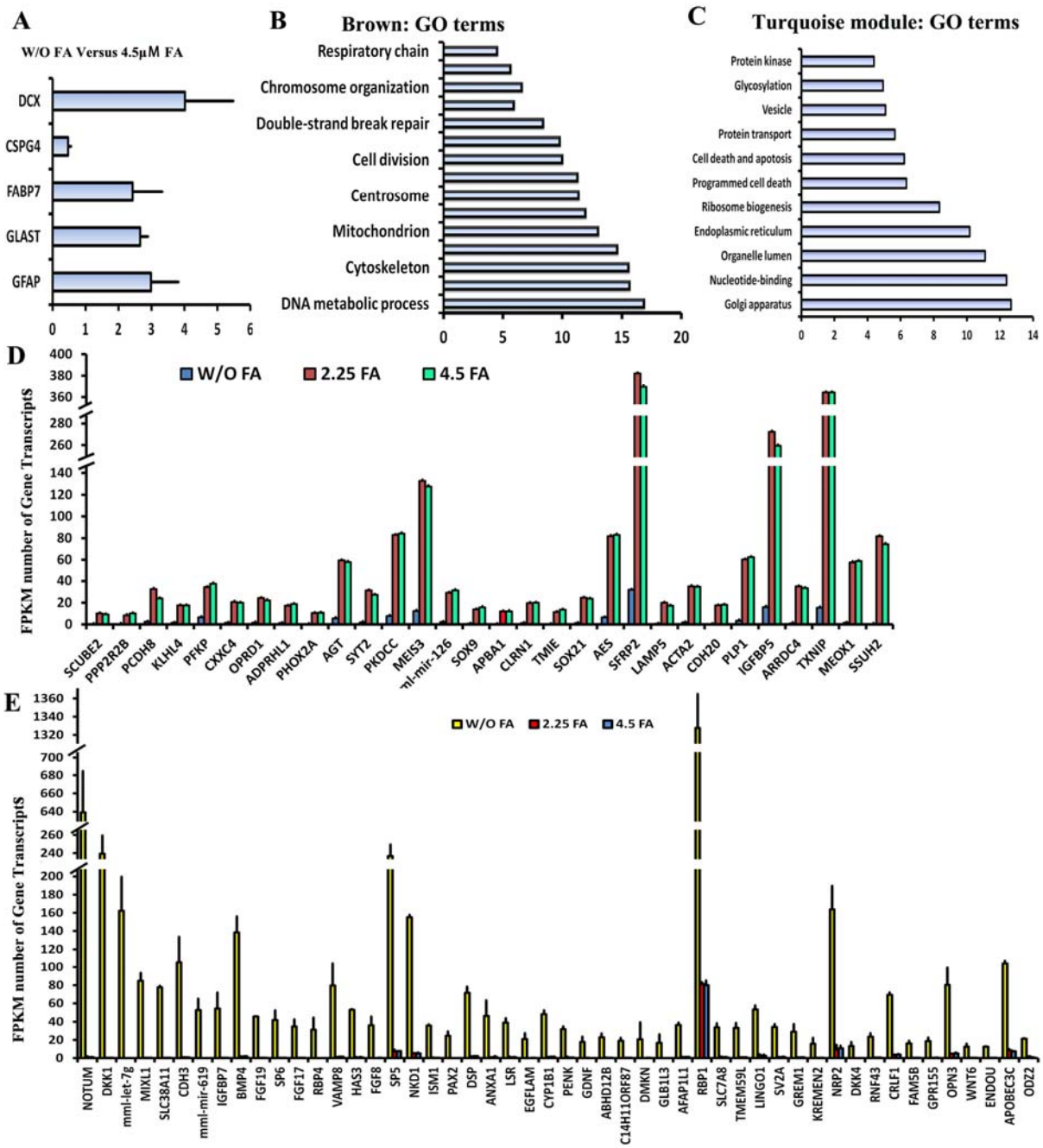
A
W/O FA Versus 4.5μM FA
DCX
CSPG4
FABP7
GLAST
GFAP
0 1 2 3 4 5 6
B
Brown: GO terms
Respiratory chain
Chromosome organization
Double-strand break repair
Cell division
Centrosome
Mitochondrion
Cytoskeleton
DNA metabolic process
0 5 10 15 20
C
Turquoise module: GO terms
Protein kinase
Glycosylation
Vesicle
Protein transport
Cell death and apotosis
Programmed cell death
Ribosome biogenesis
Endoplasmic reticulum
Organelle lumen
Nucleotide-binding
Golgi apparatus
0 2 4 6 8 10 12 14
D
W/O FA
2.25 FA
4.5 FA
FPKM number of Gene TranscriptS
SCUBE2 PPP2R2B PCDH8 KLHL4 PFKP CXXC4 OPRD1 ADPRHL1 PHOX2A AGT SYT2 PKDCC MEIS3 SOX9 APBA1 CLRN1 TMIE SOX21 AES SFRP2 LAMP5 ACTA2 CDH20 PLP1 IGFBP5 ARRDC4 TXNIP MEOX1 SSUH2
E
W/O FA
2.25 FA
4.5 FA
FPKM number of Gene TranscriptS
NOTUM DKK1 MIXL1 SLC38A11 CDH3 IGFBP7 BMP4 FGF19 SP6 FGF17 RBP4 VAMP8 HAS3 FGF8 SP5 NKD1 ISM1 PAX2 DSP ANXA1 LSR EGFLAM CYP1B1 PENK GDNF ABHD12B C14H11ORF87 DMKN GLB1L3 AFAP1L1 RBP1 SLC7A8 TMEM59L LINGO1 SV2A GREM1 KREMEN2 NRP2 DKK4 RNF43 CRLF1 FAM5B GPR155 OPN3 WNT6 ENDOU APOBEC3C ODZ2

Figure S7

**SUPPLEMENTAL FIGURE LEGENDS**

Figure S1, related to Figure 1. Rhesus monkey ES cells (rESCs) are rapidly converted into neuroepithelial stem cells (NESCs) with stable neural tube (NT) formation and neurogenic ability in large-scale expansion. Three independent experiments were repeated for NESCs from IVF3.2 and 3.3, respectively. (A) Typical EBs at post-differentiation Day 2 (pdD2); (B) EBs were organized into a neuroepithelial layer structure at pdD5. (C-E) On pdD2, 5 and 6, EBs were cryosectioned and stained with OCT4, SOX2, NESTIN and Pax6, respectively. (F) NESCs did not express TBR2, a marker of OSVZ and ISVZ progenitors in the human and primate developing cortex. These staining were independently repeated for three times. (G) Rosette structures were formed when cells were continually cultured at low cell density through Passage 3 (P3), 30 (P30) and 45 (P45). (H) The NT structures were maintained when cells were continually cultured at high cell density through P3, P30 and P45. Arrows indicate NTs. (I) The growth curve of NESCs, displaying the prospect of exponential growth over serial passages. NESCs were routinely passaged to 1:8 to 1:16 ratios every 3-4 days. (J-K) FACS data show SOX2 and NESTIN positive cells are similarly distributed and highly enriched in P18 and P36 NESCs populations. (L) Quantification of SOX2 and NESTIN positive cells in P14, P26 and P36 NESCs, respectively. Data expressed as mean±s.t.d (Data from three independent experiments) ($P>0.05$ by Student's t-test). (M) Cell cycle staining and FCAS of P18 and P36 NESCs revealed a stable population of cells in S-phase during the large-scale expansion. (N) NESCs with at least 96 population doublings display normal karyotype. Scale bar: 100μm.

Figure S2, related to Figure 2. Single neuroepithelial stem cell self-organized into neural tubes within 14 days. White arrows indicate single cell-derived colonies. On day 8, neural polarized structure began to form (red arrow). From Day 9, neural tube structure began to self-organization (white arrowheads).

Figure S3, related to Figure 1 and 2. NTs can be generated from monkey iPSCs-derived NESCs in a similar manner. Rhesus monkey skin fibroblasts from embryonic day 65 were infected with the cocktail retroviruses including *SOX2*, *OCT4*, *KLF4* and *C-MYC*. Three days after infection, fibroblasts were digested into single cells and cultured on MEFs in ESC growth media for 10-14 days. Typical iPSC colonies were picked up and subjected for passaging. iPS1.1 cell line was randomly used for pluripotent characterization and neural induction. (A) The morphology of monkey iPSCs cultured on MEFs. (B-E) Monkey iPSCs expressed

pluripotent markers, such as AP (alkaline phosphatase), OCT4, NANOG, TRA-1-81, PRDM14, TRA-1-60 and SOX2. (F) Monkey iPSCs were able to differentiate into tissues of all three germ layers, including ectoderm (neuroepithelium), mesoderm (cartilage) and endoderm (gut), when injected into SCID mouse. (G) The iPS1.1 maintained normal karyotype. (H) The morphology of monkey iPSCs-derived neural bodies at Day 5 in suspension culture. (I) The morphology of cultured Passage 5 iPSCs-NESCs at low cell density. (J) The morphology of cultured Passage 5 iPSCs-NESCs at high cell density. (K) Long-term cultured iPSCs-NESCs at passage 6 expressed stem cell markers: SOX2, PAX6, N-CADHERIN and SOX1. (L) Growth curve of iPSCs-NESCs, displaying the prospect of exponential growth over serial passages. (M-Q) Single iPSCs-NESCs self-organized into neural tubes expressing PAX6, N-CADHERIN, NESTIN and ZO-1. (R) Long-term cultured single iPSCs-NESCs gave rise to $MAP2^{+}TUJ1^{+}$ neurons. (S) Differentiated neurons from single iPSCs-NESCs were glutamergic and GABAergic neurons. Scale bars: A-C and F-G, 200 μm; D-E, 50 μm; others, 100 μm. The experiment was independently repeated for three times.

Figure S4, related to Figure 4 and 5. CHIR99021 removal resulted in rapid radial glial progenitor cell (RGPC) transition from NESCs, however, its treatment promoted newly formed RGPCs go back to the NESC state and form neural tubes. (A-H) CHIR99021 removal resulted in rapid "NESC-to-RGPC" transition. (A-F) All progenies of single NESCs were progressively converted to most of GFAP positive cells and few $TUJ1^{+}$ cells in media without CHIR99021. 10(n)/10(m) indicated that 10(n) colonies in all examined 10(m) colonies have identical phenotypes represented by the picture. (G) RNA-seq data showed NESCs in media without CHIR99021 upregulated expression of RGPC markers including *GLAST*, *CSPG4*, *FABP7* and *GFAP* at day 7. Data are from two independent experiments. (H) Experimental paradigm of CHIR99021 treatments. The CHIR99021 was added in the media from Day 0-9 (early-addition), followed by growth in media without CHIR99021 from Day 9-14 (late-withdrawal). The late withdrawal of CHIR99021 resulted in the total loss of NT formation. (I) Formed RGPCs gave rise into $TUJ1^{+}$ neurons once differentiations were induced. (J-K) Newly formed RGPCs can go back to the NESC state and form NTs upon CHIR99021 treatment. (J) Experimental paradigm of early-withdrawal (from Day 0-7, 0-9, or 0-11) followed by late-addition (from Day 7-14, 9-14, or 11-16) of CHIR99021 into the culture media. Single cells were cultured in media W/O CHIR99021 for different periods. (K) Reversed NESCs expressed PAX6, NESTIN, and N-CADHERIN, but not GFAP. (L) Addition of XAV939, a Wnt inhibitor, also completely inhibited NT formation and converted NESCs into RGPCs. Scale bar: A-F, 50μm; others, 100μm.

The experiment was independently repeated for three times.

Figure S5, related to Figure 4. NESCs have unique gene expression profiles. Gene ontology (GO) analysis for genes from different modules in Figure 4B.

Figure S6, related to Figure 4. NESCs were regionally restricted into telencephalic fate and gave rise to cortical neurons. (A) Heatmap showed NESCs and differentiated neurons highly express dorsal and ventral telencephalic markers, but negative for midbrain, neural crest and hindbrain (posterior) markers. (B) Fold upregulation changes of neuronal marker gene transcription levels in NESCs-derived differentiated neurons versus NESCs via RNA sequencing analysis. Data were from two independent experiments. (C) NESCs differentiated into $TBR2^{+}PAX6^{-}$ intermediate progenitors. (D) NESCs differentiated into $TBR1^{+}$ cortical neurons. (E-F) NESCs differentiated into II-IV upper layer $BRN2^{+}$ and $CALERETININ^{+}GABA^{-}$ cortical neurons. (G-H) NESCs differentiated into V-VI upper layer $CTIP2^{+}$ and $FOXP2^{+}$ cortical neurons. (I) NESCs were unable to differentiate into 5-HT, ChAT and TH dopamine neurons in SDM media. (J) NESCs have inability to give rise to TH dopamine neurons and HB9 motoneurons even in the specific dopamine neuron and motoneuron differentiation media. (K) Genes of published rosette-stage cells and $NSCs^{EGF/FGF}$ low or negatively expressed in NESCs, RGPCs and differentiated neurons. Scale bars: 100μm.

Figure S7, related to Figure 6 and 7. The mechanisms of NTDs caused by folic acid (FA) deficiency. (A) Down fold of expression levels of radial glial progenitor cell (RGPCs) markers in NESCs cultured in the media without FA, compared with in the media with FA. (B) Representative GO function terms of FA addition secondly upregulated brown module in Figure 6G. (C) Representative GO function terms of FA deficiency secondly upregulated brown module in Figure 6G. (D) Some representative upregulated genes induced by FA. (E) Some representative upregulated genes of NESCs in absence of FA. The data in A, D and E are two independent experiments.

**SUPPLEMENTAL VIDEO LEGENDS**

Video S1: A representative 3D reconstruction of a single cell-derived neural tube. Self-organized neural tubes by single NESCs were fixed and stained with DAPI (blue) on Day 14. A single cell-derived neural tube was scanned using a Leica TCS SP8 confocal laser scanning system. Ten neural tubes were scanned.

Video S2: Interkinetic nuclear migration (IKNM) in single cell-derived neural tubes. Live imaging of retrovirus GFP infected NESCs revealed movement of nuclei along apical and basal surface. Arrows mark two NESCs in particular with clear IKNM. Horizontal divisions (0-30°, spindle orientation) were close to apical side in NTs. Time shown in hrs: min.

SUPPLEMENTAL TABLE LEGENDS

Table S1

The gene list of GO terms for different module in supplemental Figure 5.

Table S2

The gene list of GO terms for different module when NESCs cultured in the media without folic acid, or with 2.25 μM or 4.5 μM folia acid, respectively. The GO terms are relative to Figure 7 and Supplement Figure 6.

## SUPLEMENTAL EXPERIMENTAL PROCEDURES

### Embryonic stem cell culture and neuroepithelial stem cell (NESC) induction

IVF3.2 and IVF3.3 rhesus monkey embryonic stem cells (rESCs), and monkey fibroblast-derived iPS line 1.1 were cultured on X-ray inactivated CF-1 mouse embryonic fibroblasts (MEFs) in ESCs growth media [DMEM/F12 (1:1) (Invitrogen) containing 15% KSR (Invitrogen) and 5ng/mL bFGF (Millipore)] (Li et al., 2005; Sun et al., 2011). The monkey fibroblast-derived iPS line 1.1 was obtained by the modified protocol (Liu et al., 2008). Briefly, skin fibroblasts were obtained from one male rhesus monkey fetuses of embryonic 65 days. Plasmids pMX-*OCT4*/*SOX2*/*KLF4*/*C-MYC* 6μg, pCL6μg were prepared to transfect 293T cells by the $Ca_3(PO4)_2$ method. 12 hours after transfection, the medium was changed. 48 hours after transfection, virus-containing supernatants were collected, filtered through a 0.45 μm pore-size filter and concentrated by 5-fold for use. The four concentrated retroviruses were mixed to infect monkey fibroblasts which were passaged 24 hours before at $3\times10^4$ cells per 35mm dish. At the first day after infection (piD1), infected fibroblasts were infected by the four concentrated retroviruses again. About 80% of fibroblasts were routinely infected by any one of OCT4, SOX2, KLF4 or C-MYC viruses. At piD3, infected fibroblasts were digested into single cells and cultured on MEFs in ESCs growth media. 10-14 days after infection, typical iPSC colonies were mechanically picked up and subjected for passaging. One cell line iPS1.1 was randomly used for pluripotent characterizations and the following neural induction.

ESCs or iPS1.1 were digested with Collagenase IV (Gibco) and neural induction was induced by switching from ESC growth media to differentiation media in suspension culture [Advance DMEM/F12 (1:1) (Invitrogen): Neurobasal media (Invitrogen) (1:1 mixture) supplemented with 1xN2 (Invitrogen), 1xB27 (Invitrogen), 10ng/ml bFGF (Millipore), 3μM CHIR99021 (Cellagen technology), 5μM SB431542 (Cellagen technology), 0.2 μM Compound E and 0.1μM LDN193189 (Cellagen technology)]. After 6 days,

EBs were transferred to 5μg/ml laminin (Gibco)-coated plates for attachment culture and the media was switched to NESCs culture media [Neurobasal media including 1xB27, 1xN2, 1XNEAA (Sigma), 1% Glutmax (Sigma), 3 μM CHIR99021, 5μM SB431542, 10ng/ml bFGF, and 1000U/ml hLIF (Millipore)].

**Culture and large-scale expansion of NESCs**

Neuroepithelial stem cells (6 days after EB differentiation of ESCs) were cultured on 5μg/ml laminin (Gibco) coated plates in NESCs culture media (detailed above). 0.025％ trypsin (Sigma) was used to digest NESCs when passaging to encourage cell propagation. NESCs were routinely passaged to 1:8 to 1:16 ratios every 3-4 days. For NT formation, NESCs were continually cultured 8-10 days before passaging.

**NESC differentiation**

For spontaneous differentiation, NESCs were cultured on laminin (5μg/ml) and gelatin (0.05%) coated plates in differentiation media (SDM) [Neurobasal supplemented with 1xN2, 1xB27, 1XNEAA and 1% Glutmax]. On Day 6, 10ng/ml BDNF (R&D systems) and 10ng/ml GDNF (R&D systems) were added into the media to induce terminal maturation of neurons. For GABAergic neuron differentiation, 10 ng/ml SHH (R&D Systems) was added into the differentiation media for the first 4 days. On Day 5, 10ng/ml BDNF (R&D systems) and 10ng/ml GDNF (R&D systems) were added into the media to induce terminal maturation of neurons. For density differentiation experiments, the differentiations were induced at $9.5x10^3$ cells/$cm^2$ for high cell density differentiation and at 2.1 $x10^3$ cells/$cm^2$ for low cell density differentiation, respectively.

To induce dopaminergic neuron differentiation, NESCs was first cultured in the SDM media including 500ng/ml SHH (R&D Systems), 500 ng/ml FGF8 and 4μM purmorphamine for 7 days, following in the dopamine neuron matured media including 10ng/ml GDNF, 10 ng/ml BDNF, 10ng/ml IGF and 0.5 mM db-cAMP for another 10 days.

For motoneuron differentiation, NESCs were treated by the SDM media surplus with 200 ng/ml SHH and 1μM RA (retinoic acid) for 7 days. To facilitate the maturation of differentiated neurons, the differentiated cells were also treated with 10ng/mL BDNF and 10ng/mL GDNF for additional 2-3 weeks.

**Immunocytochemistry and flow cytometry**

For immunocytochemistry, cells were fixed with 4% paraformaldehyde for 15 mins, washed with PBS, treated with 0.1% Triton X-100 (Invitrogen) for 20 mins, washed three times with PBS, and incubated in blocking buffer (0.1% Tween 20 and 10% normal donkey serum (Invitrogen) in PBS) for 30 min at room temperature. The cells were incubated with primary antibody overnight at 4 $^{o}$C. Primary antibodies are listed in the following: TUJ1 (Covance, MRB435P, 1:1000); TUJ1 (Millipore, MAB1637, 1:1000); TBR2 (Millipore, AB2283, 1:300) ; TH (Millipore, AB152, 1:400); Cholinergic (ChAT) (Millipore, AP144P, 1:600); HB9 (Millipore, ABN174,1:500 ); SOX2 (Millipore, MAB5603, 1:400); NESTIN (Millipore, MAB5922, 1:400); MAP-2 (Millipore, MAB5622, 1:600); SYNAPSIN I (Sigma, S193, 1:500); GFAP (Sigma, G9269, 1:2000); BrdU (Sigma, B8434, 1:300); GABA (Sigma, A2052, 1:600); vGLUT1 (Sigma, V0389, 1:1000); SEROTONIN (5-HT) (Sigma, S5545, 1:1500); P-VIMENTIN (MBL International, D076-3S, 1:200); PAX6 (RD, MAB1260, 1:1000); SOX1 (R&D, AF3369, 1: 400); PSD95 (ABCAM, ab2723, 1:300); GFP (Abcam, ab13970, 1:1000); OCT4 (Santa Cruz, SC5279, 1:400); N-CADHERIN (Santa Cruz, SC7939, 1:50) and ZO-1 (Invitrogen, 339100, 1:50). The following day, the cells were washed with PBS and incubated with Alexa488 or rhodamine-conjugated secondary antibodies (Invitrogen: goat-anti-rabbit, goat-anti-mouse**,** donkey- anti-goat**,** donkey-anti-chicken, 600×) in PBS for one hour at RT. Nuclei were visualized with DAPI staining (Sigma-Aldrich). For BrdU staining of NTs, NESCs with typical NTs were treated with 5 μ g/ml Bromodeoxyuridine (Sigma) for 0.5 hr (NESC-derived colonies) or 1.5 hr

(single cell-derived colonies) and then fixed with 4% paraformaldehyde. To test the effect of folic acid (FA) on proliferation of NESCs, 5μg/ml BrdU were added into the media for 0.5h after NESCs were cultured in the media without FA, or with 2.25μM FA or 4.5μM FA for three days, respectively. Fixed cells were treated with 0.1% Triton X-100 for 20 min, followed by 1M HCL for 30 min at 45℃.

For indirect flow cytometry, cells were incubated with mouse anti-Nestin and rabbit anti-Sox2 for overnight at 4°C and washed three times with PBS. Cells were then incubated with Fluor 488 or rhodamine conjugated goat anti-rabbit IgG and Fluor 488 or rhodamine conjugated goat anti-mouse IgG (Invitrogen, 1:1,000) for 30 min on ice and washed three times. Cells directly incubated with secondary antibody were used as control. Cell cycle assays were performed following the instructions of the Cell Cycle Kit (Beyotime). Flow cytometry analysis was carried out with a FACScan flow cytometer (BD Biosciences).

**RT-PCR**

RNA was isolated with Trizol reagent according to the manufacturer's instructions (Invitrogen). cDNA was reserved with the M-MLV first strand kit (Invitrogen) according to the manufacturer's protocol. The primers for *OCT4*, *SOX2*, *PAX6* and the house-keeping gene *GAPDH* are the following: *OCT4*-F, 5'-GTTCAGCCAAACGACCATC-3'; *OCT4*-R, 5'-GGAAAGGGACCGAGGAGTAC-3'; *SOX2*-F, 5'-AGAGTGGAAACTTTTGTCGG-3' , *SOX2*-R, 5'- GGAGTGGGAGGAAGAGGTAA-3'; *PAX6*-F, 5'-CCCGTCCATCTTTGCTTG-3', *PAX6*-R, 5'- TCATAACTCCGCCCATTCA-3'; *GAPDH*-F, 5'-GCATCAACAGCAGCATCGAGAAC-3', *GAPDH*-R, 5'-CTCCATTTGGCCCTTAACTTG-3' .

**Single cell clone assays**

Single NESCs were diluted to approximately 1000 cells/ml and 1 μl of these cell suspensions were seeded into NESCs media in individual wells of 96-well plate coated with laminin (5 μg/ ml). Wells containing only one cell were confirmed and wells with multiple cells were excluded by visual observation under microscopy 4 hours after seeding. After seeding, the media was replaced with fresh media every 2-3 days until Day 14. The NT colonies were counted under ZO-1 staining, respectively.

**Electrophysiology**

For electrophysiological recording, matured cells derived from P31 NESCs were cultured on coverslips for 26 days and were placed in a recording chamber continuously superfused with oxygenated artificial cerebral spinal fluid (mACSF) under a Olympus BX50WI upright infrared DIC microscope. The mACSF was composed of 119mM NaCl, 2.5mM KCl, 26mM $NaHCO_3$, 1mM $NaH_2PO_4$, 11mM Glucose, at pH 7.4, 300 mOsm. Patch clamp recording pipettes with resistance of 4-8 M were pulled using the laser based P-2000 micropipette puller (Sutter Instrument). Whole cell recording was conducted using the Multiclamp 700A amplifier (Molecular Device) with a 10 KHz sampling rate and were low-pass filtered at 1KHz for current clamp recordings. The pipettes were filled with an intracellular solution containing 130mM KCl, 2mM MgCl2, 10mM KOH, 1mM EGTA, 10mM HEPES, 5mM ATP, and 0.3mM GTP (pH 7.2). During current clamping, the current was held to 0 pA (I=0). For current injection steps, ten sweeps were made at each 20 pA increments from -60 to 120 pA. Changes in spike frequencies were calculated by subtracting resting frequencies from those measured with the current injection. Sodium currents were recorded in voltage clamp mode. All reagents were obtained from Sigma.

**RNA Sequencing (RNA-Seq) and gene expression analysis**

Total RNA was extracted from five different samples of cells at different stages using the RNAeasy

Micro Kit (Qiagen). The samples included P5 NESCs, P24 NESCs and P36 NESCs, P36 NESC-DN (P36 NESCs had been spontaneously differentiated for 13 days) and induced RGPCs (NESCs cultured in NESC media without CHIR99021 for 7 days). mRNA samples were purified using Oligotex Direct mRNA Kits, according to the manufacturer's instructions (Qiagen). 500 ng mRNA of each sample was used to produce its respective sequence library. mRNA was fragmented using the fragmentation Buffer (Ambion) and double-stranded cDNA was then synthesized using SuperScript II (Invitrogen) RT and random primers. Sequencing was then performed in a HiSeq 2500 apparatus (Illumina) according to the TruSeq RNA Sample Preparation Guide (Illumina). RNA sequencing was performed with the paired end 2x100nt multiplex program. The whole sequencing process was controlled by the Data Collection Software. At least 20M raw reads were taken for every sample. All reads were then mapped using the reference of ensemble macaca_mulatta MMUL_1.72. Mapping ratios of all samples were higher than 90%. Over 16,971 genes were detected with expression in at least one sample. Gene expression analysis was performed by the following methods. Scaled expression levels were used to visualize the expression profiles via heatmap. All transcripts were clustered into 10 modules using k-means. Module names were converted to color names by an R package "WGCNA" (Langfelder and Horvath, 2008). Module functions were analyzed via Database for Annotation, Visualization and Integrated Discovery (DAVID). Based on WGCNA, module eigengenes (MEs) that represent the first principle component of one module were calculated, and related MEs to cell types were used to investigate cell-type related gene modules. To reveal hub genes of a module, the intra-module connectivity were calculated, and the top 30 highly connected genes in each module were defined as hub genes. The coexpression network of hubgenes and functional related genes was visualized via ViSANT software.

For FA dependence experiments, NESCs were digested into single cells and $5.0x10^4$ cells/well were

replated on laminin-coated 6-well plates. The NESCs media were changed into RPIM 1640 NESCs media without FA or with 4.5 μ M FA on the next day, respectively. After 8 days, NESCs were collected to purify RNA, respectively. Two replicates were independently performed. RNA sequencing was then performed based on the above-mentioned protocol. Transcript abundances were quantified using Cufflinks 2.2.1. ~15000 genes were detected with expression in at least one sample. Among which, ~13000 genes were detected with average FPKM>0.1. To evaluate the overall similarity in gene expression, a data matrix of log-transformed the above FPKM values were used for sample-wise hierarchical clustering. The hierarchical clustering analysis was performed using average linkage method and Pearson's correlation as the distance metric. Differential Expression Analysis was performed with linear models as implemented in Limma R package to call significant differentially expressed genes between folic acid treated and untreated cells. ~6000 genes with adjust P value <0.05 were used for the following K-means analysis using Cluster 3.0 to reveal the different clusters or modules of genes with similar gene expression patterns. Euclidean distance was used as the similarity metric. Java tree View was used for the cluster graphing. The Database for Annotation, Visualization and Integrated Discovery (DAVID) was then used to identify enriched Gene Ontology terms within each cluster or module identified by K-means analysis.

**Live imaging of NESCs interkinetic nuclear migration in a single cell-derived NT**

Replication-defective retrovirus encoding a GFP was produced by co-transfecting a retroviral vector (pMx-GFP from Addgene) with the packaging plasmid pCL (Imgenex, San Diego) in 293T cells. Single NESCs-derived colonies at Day 7 were infected with a retrovirus containing pMx-GFP vector for 4 hours. Then, the media was replaced with fresh NESCs culture media. Live imaging was performed using a Leica TCS SP8 confocal laser scanning system (Leica) equipped with 37$^{o}$C temperature and 5% $CO_2$ control. Day 14 single NESCs-derived colonies with NT structures containing GFP-positive cells were imaged with a

40× objective. Time-lapse images were captured at 4 min intervals for 5–10 h.

**Cell transplantation**

To obtain single NESC-derived cell lines labeled by GFP, NESCs were infected by lentivirus containing GFP and performed clonal expansion. Single-derived GFP positive colonies were selected to continually expand. Four GFP positive cell lines were established and one cell line was randomly chosen for following transplantation.

All surgical procedures and manipulation processes were conducted according to guidelines of the Use and Care of Experimental Animals of the International Association for Assessment and Accreditation of Laboratory Animal Care (AAALAC) and the Kunming Biomed International Animal Care Committee. Two new born health cynomolgus monkeys (about one month, male), with a body weight ranged from 500 to 800g, were used in the present study. Monkeys were firstly anesthetized with katamine (10 mg/kg) and pentobarbital (10 mg/kg), following preanesthetic medication of atropine (0.1mg/kg) and morphine (0.5mg/kg). They were then placed into a monkey stereotaxic instrument for surgery. Both monkeys underwent a single surgery with a intracranial unilateral injection of single cell-derived NSECs cells labeled by GFP. The unilateral injection was performed in left visual cortex (10μL, $2x10^5$ cells per μL). After surgery, monkeys were given antibiotics for 1 week. Each monkey was housed with his mother in one cage, respectively. The light/dark cycle for these new-born monkeys is 10h/14h.

**Tissue processing**

Animals were euthanatized with Katamine (10 mg/kg) and pentobarbital (100 mg/kg) before cardiac perfusion with 0.01M PBS. Fresh cold 4% PFA was used to perfuse the monkey (Sigma, PH7.4). Brains were then extracted, post-fixed in 4% PFA (2-3 days) and dehydrated in sucrose solution (10%, 20% and 30%, respectively). The transplanted sites were eventually sectioned on a cryostat microtome at 20μm after

embedding in O.C.T (Sakura-Finetek) and stained with GFP and the neuron or astrocyte antibodies (See Supplemental Table 1). Based on the original sites of injection, cell migration and axon outgrowth in brain sections was measured with a microscale. Every four sections, one section was used to examine GFP cells and stained with neuronal antibodies. The proportion of GFP-labeled cells stained with lineage-specific phenotype markers and a nuclear label (DAPI) was determined by Leica SP8 confocal microscopy. Two thousands or more cells were scored for each marker, such as NeuN, GFAP, vGLUT1 and GABA.

**Statistical analysis**

All of experiments including immunohohistochemistry were at least performed triplicates. For quantifying neurons, TUJ1 positive cells with a neuronal morphology (a circular, three-dimensional appearance that extend a thin process at least three times longer than their cell body) were quantified as neurons after 2 weeks of differentiation. Quantification was performed on randomly selected 5-8 pictures taken under Leica microscopy using the Leica software package and at least one thousand cells were counted for every experiment. All quantifications are based on at least three independent experiments. Quantification data represented as mean ± standard deviation (s.t.d) using Microsoft Excel STDEV Function. The significance difference between two samples was evaluated by the unpaired two-sample Student's *t*-test using Excel software. $P<0.05$ was considered as statistical significant differences.

**SUPPLEMENTAL REFERENCES:**

Langfelder, P., and Horvath, S. (2008). WGCNA: an R package for weighted correlation network analysis. BMC Bioinformatics *9*, 559.

Li, T., Wang, S., Xie, Y., Lu, Y., Zhang, X., Wang, L., Yang, S., Wolf, D., Zhou, Q., and Ji, W. (2005). Homologous Feeder Cells Support Undifferentiated Growth and Pluripotency in Monkey Embryonic Stem Cells. STEM CELLS *23*, 1192-1199.

Sun, Z., Wei, Q., Zhang, Y., He, X., Ji, W., and Su, B. (2011). MicroRNA profiling of rhesus macaque embryonic stem cells. BMC genomics *12*, 276.